INFORMATION TO USERS

This manuscript has been reproduced from the microfilm master. UMI films the text directly from the original or copy submitted. Thus, some thesis and dissertation copies are in typewriter face, while others may be from any type of computer printer.

The quality of this reproduction is dependent upon the quality of the copy submitted. Broken or indistinct print, colored or poor quality illustrations and photographs, print bleedthrough, substandard margins, and improper alignment can adversely affect reproduction.

In the unlikely event that the author did not send UMI a complete manuscript and there are missing pages, these will be noted. Also, if unauthorized copyright material had to be removed, a note will indicate the deletion.

Oversize materials (e.g., maps, drawings, charts) are reproduced by sectioning the original, beginning at the upper left-hand corner and continuing from left to right in equal sections with small overlaps. Each original is also photographed in one exposure and is included in reduced form at the back of the book.

Photographs included in the original manuscript have been reproduced xerographically in this copy. Higher quality 6" x 9" black and white photographic prints are available for any photographs or illustrations appearing in this copy for an additional charge. Contact UMI directly to order.

UMI

A Bell & Howell Information Company
300 North Zeeb Road, Ann Arbor MI 48106-1346 USA
313/761-4700 800/521-0600

Université d'Ottawa · University of Ottawa

MODELLING OF A HOLLOW FIBRE BIOARTIFICIAL LIVER AND PANCREAS

By

©Marc Paris

A thesis submitted in partial fulfilment
of the requirements for the degree of

Master of Applied Science

in the

DEPARTMENT OF CHEMICAL ENGINEERING
UNIVERSITY OF OTTAWA

Ottawa, Canada

November 10th, 1997

Research director: Dr. David Taylor

Candidate: Marc Paris

Although the human spirit has been the basis of numerous discoveries, it will never invent anything as beautiful, as simple or as direct as anything created by nature, where nothing is missing or superfluous.

Leonardo da Vinci

I would like to thank Dr. David Taylor, professor at the University of Ottawa, for the indispensable guidance and encouragement he supplied throughout all stages of this research project.

I would also like to thank the National Sciences & Engineering Research Council of Canada for their funding.

ABSTRACT

In the last two decades, significant advances in the development of bioartificial organs have been achieved. In particular the hollow fibre bioreactor has demonstrated enormous potential as a possible bioartificial organ.

Although considerable study has been conducted, the field of process modelling, particularly in the case of the bioartificial liver, has generally been neglected. A one-dimensional model was therefore developed to predict the performance of the hollow fibre bioartificial pancreas and liver. The impact of bovine serum albumin polarisation in the fibre's extra capillary space on device performance was evaluated.

The simulations conducted for the bioartificial pancreas showed that protein polarisation can significantly reduce device performance when the system relies on convective mass transport across the membrane.

In the case of the bioartificial liver, protein polarisation resulted in an apparent reduction of ammonia and n-caproic acid consumption. Most of the performance increase observed for a system where no protein was present is due to species accumulation in the extra capillary space. The convective flux of ammonia and n-caproic acid across the membrane particularly improved device performance during start-up conditions.

RÉSUMÉ

Les deux dernières décennies ont témoigné du développement accéléré des organes bioartificiels. Un de ces procédés : le bioréacteur à fibres creux a fait preuve d'énorme potentiel en tant qu'organe artificiel.

Bien que de nombreuses études aient été faites, la simulation mathématique de ces procédés, le foie artificiel en particulier, a été négligée. Un simulateur numérique à une dimension a donc été développé afin de prédire la performance d'un pancréas et foie bioartificiel à fibres creux. L'impact de la présence de l'albumine, situé dans l'espace vide inter-capillaire, sur la performance de l'organe artificiel a été évalué.

Les simulations obtenues pour un pancréas bioartificiel ont démontré que la polarisation des protéines peut considérablement réduire la performance des systèmes où l'échange des composés se déroule surtout par convection.

La polarisation des protéines dans le cas du foie artificiel a entraîné une réduction apparente de la performance du système. Presque toute l'augmentation de la consommation d'ammoniaque et d'acide caproique observée durant l'opération du système dépourvu de protéine a été causée par l'accumulation de ces substances dans l'espace inter-capillaire. Le transport par convection a particulièrement augmenté la performance du système durant les conditions de démarrage.

TABLE OF CONTENTS

LIST OF FIGURES

LIST OF TABLES

NOMENCLATURE

Variable	Definition
A_2	Virial coefficient (m^3 / kg)
A_3	Virial coefficient (m^6 / kg^2)
a_E	Eastern control volume coefficient (m / s)
a_P	Central control volume coefficient (m / s)
a_W	Western control volume coefficient (m / s)
C	Concentration (kg / m^3 or mol / m^3)
c	Cell viability
D	Diffusivity (m^2 / s)
F	Convective transport term (m / s)
J	Species flux (mol / m^3 s)
K_c	Death rate constant (1 / s)
$K_{n\text{-}cap}$	n-caproic acid metabolic rate constant (m3 / cell s)
K_{NH4}	Ammonia metabolic rate constant (m^3 / cell s)
L	Hollow fibre length (m)
L_P	Membrane hydraulic permeability (m)
M	Molecular weight (Dalton)
N_0	Cell density (alive and dead) (cells / m^3)
P	Pressure (Pa)
Peclet	Peclet number
p_M	Membrane species permeability (m / s)
r	Radius (m)
R	Ideal gas constant (Pa m^3 / mol °K)
Rct	Reaction rate term (mol / m^3 s)
S_C	ϕ independent source term (units of ϕ / m^3 s)
S_P	ϕ dependent source term (1 / s)
t	Time (s)
T	Absolute temperature (°K)
t_1	First time delay constant (s)
t_2	Second time delay constant (s)
u	Axial velocity (m / s)
V	Velocity vector
v	Radial velocity (m / s)
x	Control volume width (m)
z	Axial position (m)

NOMENCLATURE (Continued)

Greek Variable	Definition
Γ	Diffusive transport term (m / s)
Π	Osmotic pressure (Pa)
α_1	First inverse time constant (1 / s)
α_2	Second inverse time constant (1 / s)
ϕ_E	Eastern control volume variable (units of ϕ)
ϕ_P	Central control volume variable (units of ϕ)
ϕ_P^0	Previous time step's ϕ value (units of ϕ)
ϕ_W	Western control volume variable (units of ϕ)
μ	Fluid viscosity (Pa s)
ν	Kinematic viscosity (m^2 / s)
θ	Angular component (radians)
σ	Reflection coefficient
ξ	Geometric factor

Subscript	Definition
–	Bar above variable indicates a radially averaged value
0	Lumen inlet
1	Inner membrane
2	Outer membrane
3	Krogh cylinder boundary
E	Extra capillary space
e	Eastern control volume face
init	Value at time 0
L	Lumen
M	Membrane
P	Central node
w	Western control volume face

Chapter 1

Introduction

1.1 Organ Transplants

Tissue loss and end-stage organ failure are some of the most important medical problems facing our national health care system (see Table 1.1.1). The health care bill in the United States alone exceeds $400 billion dollars annually and approximately 8 million surgical procedures are required (Langer & Vacanti 1993). In many situations, such as liver failure, whole organ transplantation remains the only clinically effective solution (Rozga & Demitriou 1995).

In the latter half of the twentieth century, the field of organ transplantation has undergone incredible improvement. Despite the progress, a number of difficulties still remain. Chief among them is the shortage of donated organs. Many patients die while waiting for an available organ. In the case of liver failure only one donor is available for every ten patients (Langer & Vacanti 1993). In addition to the lack of viable organs, many transplantation procedures also suffer from a relatively high morbidity rate. Further, transplant patients often require life-long immunotherapy. Finally, transplant procedures are generally quite expensive.

Because of these difficulties, a number of alternatives to whole-organ transplantation are actively being pursued. Purely mechanical methods such as dialysis have long been developed to help alleviate certain physiological deficiencies. Although these techniques have proved themselves extremely valuable, a new breed of hybrid devices shows great promise as alternatives to transplantation. These bioartificial organs incorporate a mechanical and a biological component. In the following sections, the current status of mechanical and bioartificial solutions to kidney, pancreas and liver deficiencies will be discussed.

Table 1.1.1: Incidence of organ and tissue deficiencies or the number surgical procedures related to these deficiencies in the United States (Langer & Vacanti 1993)

Deficiency	Procedures or Patients per year
Skin	
Burns	2,150,000
Pressure sores	1,500,000
Venous statis ulcers	500,000
Diabetic ulcers	600,000
Neuromuscular disorders	200,000
Spinal cord and nerves	40,000
Bone	
Joint replacement	558,200
Bone graft	275,000
Internal fixation	480,000
Facial reconstruction	30,000
Cartilage	
Patella resurfacing	216,000
Chondromalacia patellae	103,400
Meniscal repair	250,000
Arthritis (knee)	149,900
Arthritis (hip)	219,300
Fingers and small joints	179,000
Osteochondritis dissecans	14,500
Tendon repair	33,000
Ligament repair	90,000
Blood vessels	
Heart	754,000
Large and small vessels	606,000
Liver	
Metabolic disorders	5,000
Liver cirrhosis	175,000
Liver cancer	25,000
Pancreas (diabetes)	728,000
Intestine	100,000
Kidney	600,000
Bladder	57,200
Ureter	30,000
Urethra	51,900
Hernia	290,000
Breast	261,000
Blood transfusions	18,000,000
Dental	10,000,000

1.2 Kidney

Kidney dialysis is commonly considered the grandfather of all artificial organs. By using a machine to perform the kidney's main filtering function, a new approach to treating physiological deficiencies was established. In dialysis, blood is pumped past a semi-permeable membrane and toxins and waste products are removed from the blood stream (Ronco 1994, Cieslinski & Humes 1994, Langsdorf *et al.* 1993, Zydney 1993, Fitzgibbons 1994).

The original dialysis membrane was no more than a commercially available sausage casing (Lysaght 1995). During the 40s and 50s regenerated cellulose was the material of choice, but it has given way to cellulose triacetate, polysulfone, polyethersulfone and polyamide (Lysaght 1995). These materials have allowed the development of much thinner membranes thereby improving the dialysis.

Changes in device geometry also significantly improved its performance. The first devices were rotating drums but these were quickly replaced by a flat plate or a twin coil design (Lysaght 1995). These were in turn supplanted by hollow fibre devices, reducing stagnant and slow moving layers that exhibited poor mass transfer. The hollow fibre design also offered the advantage of a greatly increased surface area to volume ratio.

The imposed method of solute transport during dialysis has also evolved in the last fifty years. Original devices relied solely on diffusive mass transfer to remove toxins and waste products. In conjunction with ultrafiltration membranes, forced convection can significantly improve device performance. When convection is the predominant transport mechanism a larger proportion of high-molecular weight proteins are removed. This behaviour mimics that of the native kidney's glomerulus (Cieslinski & Humes 1994).

Although dialysis proved to be an important first step to which at least a million people owe their lives, it is far from ideal. Patients must be connected to a machine at least 12 hours a week and must follow strict diets (Fitzgibbons 1994). The dialysis machine responds to changes in patient condition only with the help of an extensive infrastructure. Blood pressure and composition must be monitored and synthetic hormone injections are required to replace lost kidney function (Fitzgibbons 1994).

In order to develop the ideal artificial kidney, its functionality beyond that of a simple filter should be considered. It is known that the kidney converts vitamin D to a component that regulates the absorption of calcium (Fitzgibbons 1994). When this functionality is absent, the calcium level in the blood drops and it must be absorbed from the bones, eventually leading to bone disease. The kidneys also regulate the oxygen level in the blood by producing the hormone erythropoietin (Fitzgibbons 1994). Dialysis patients commonly suffer from anaemia and blood transfusions become necessary.

These difficulties have led some researchers to develop alternatives to dialysis. These new approaches would not only provide the ultrafiltration that is present in dialysis but would also provide the homeostatic regulatory and endocrine functionality of the native kidney. This could be accomplished with a two-stage device. The first stage, a bioartificial glomerulus would provide the ultrafiltration capability of the device. To improve long-term hemocompatibility and hemofiltration in vivo, endothelial-cell seeded conduits and filtration surfaces could be used (Cieslinski & Humes 1994, Kadletz *et al.* 1992, Schnider *et al.* 1988, Shepard *et al.* 1986).

A bioartificial tubule could provide the remaining kidney functionality. This would involve a combination of living cells supported on a polymeric matrix. By using an appropriate membrane, immunoisolation and long term cell viability can be assured. A sufficient number of progenitor cells with the ability to differentiate could provide a replacement for renal tubule function (Cieslinski & Humes 1994, Aebischer *et al.* 1991, Ip & Aebischer 1989).

The combination of a bioartificial glomerulus and tubule could take the form of either an extracorporeal or an implantable device.

The above background information was included because the artificial kidney was the precursor to all other artificial organs. However, the simulations included in this thesis only investigated bioartificial pancreas and liver operation and performance.

1.3 Pancreas

Diabetes is the third leading cause of death in the United States. Every year, over 728,000 new cases of diabetes, resulting from pancreatic insufficiency, are diagnosed in the United States. The total cost is estimated at over $20 billion annually (Langer & Vacanti 1993).

The pancreas is composed mostly of acinar cells that secrete digestive enzymes into the small intestine. One to two percent of the mass is composed of islets of Langerhans that secrete various hormones including insulin that drain into the liver. When the blood glucose concentration rises, the beta cells in the islets secrete insulin. Insulin acts on cell receptors and increases the level of glucose uptake.

A diabetic patient's insulin secreting ability is either impaired or destroyed altogether. Some of the complications that result from the ensuing hyperglycemia include heart disease, stroke, blindness, kidney disease and gangrene (Jarret & Keen 1976). There are two classes of diabetes. Type I diabetes occurs in about 5 to 10 percent of the cases and is the most severe (Colton & Avgoustiniatos 1991). It is an autoimmune process mediated by islet cell antibodies and / or lymphocytes that selectively destroy the islets (Reach 1995). Meanwhile, Type II diabetes, also known as non-insulin dependant diabetes, occurs in the remainder of the diabetic population. Only a small number of these diabetics require insulin injections.

Several potential treatments for diabetes have been developed. They can be classified into three groups: mechanical solutions, allogeneic islet transplantation and hybrid devices.

Mechanical Solutions

Although insulin injections are undoubtedly a major advance in the treatment of diabetes, they are not a perfect solution. Aside from their inconvenience, there is a real danger of injecting too much or too little insulin. Patients suffering from extreme hypoglycemia may fall into a coma and die. Injections do not deliver insulin in a steady, controlled fashion and this increases the possibility of glycemic excursions. Some researchers have postulated that it might be possible to develop a chemical or mechanical glucose sensor and insulin delivery system. The ideal device could be implanted and would respond automatically to an increase in blood glucose concentration.

Some work has been done to synthesise a gel-like material whose pore size could respond reversibly to a change in pH (Reach 1995). Insulin would be entrapped within the gel. Glucose-oxydase, meanwhile, would also be implanted in the gel layer. This enzyme will oxidise glucose and produce an acid, thereby lowering the pH. A low pH would, in turn, increase the pore sizes and release more insulin.

Another alternative involves combining a continuous blood glucose monitor with an insulin pump. A computerised control system could automatically adjust the pump's flow rate in response to a varying glucose concentration. Extra-corporeal and implantable pumps have already been developed. The primary difficulty lies in the development of a reliable implantable glucose sensor (Reach 1995, Reach 1994, Pillarella & Zydney 1990a). The most likely candidate would also be based on glucose-oxydase. The oxidation of glucose yields hydrogen peroxide that can decompose in the presence of an electric potential. The electric field that is generated could then be correlated to the glucose concentration (Reach 1995).

Allogeneic Islet Transplantation

A second alternative to the treatment of diabetes involves a purely biological solution. Attempts have already been made to inject human islets into the portal vein of diabetic patients (Scharp *et al.* 1991). Up to 14,000 islets per kilogram of body weight have been injected into seven patients. Although immunosuppressive drugs were required, one of the patients attained insulin independence for over 120 days. In addition, islet functionality was observed 10 months after implantation.

Although these results are extremely encouraging, two main difficulties remain – the requirement of long term immunosuppression and the availability of donor cells. To prevent outright tissue rejection, allogeneic cells must be used. Unfortunately, the lack of organ availability that plagues almost every type of organ transplantation procedure is a sad reality in the case of islet transplantation as well. While previous canine studies initially indicated that 5,000 islets / kg of body weight would be sufficient (Warnock & Rajotte 1988), nearly twice the number is actually required to achieve insulin independence (i.e. over 10,000 islets / kg of body weight). Any significant immune response or cell death rate would certainly make periodic "booster" injections necessary. However, if it were possible to inject animal cells without provoking an immune response, both the problem of immunosuppression and that of cell availability would be solved.

Hybrid Devices

A third alternative that attempts to combine the best of both worlds is being developed. These bioartificial organs come in various flavours but the two most common ones are the hollow fibre bioreactor and microcapsules.

A hollow fibre bioreactor is similar to a shell and tube heat exchanger. A bundle of hollow semi-permeable fibres made of polymeric material are contained in a plastic shell. The fibres are potted at both ends. The fluid flowing through the lumen is

therefore isolated from the fluid in the extra-capillary space (ECS). A diagram of a typical hollow fibre bioreactor is presented in Figure 1.3.1.

Xenogeneic islets are located in the ECS. The pores in the hollow fibres are sized to exclude immune factors while allowing free passage to nutrients and insulin. The glucose can penetrate the ECS and stimulate the insulin production. The insulin then re-enters the lumen and is delivered to the rest of the body. To obtain an adequate pressure drop, the device must be connected as an artero-venous shunt.

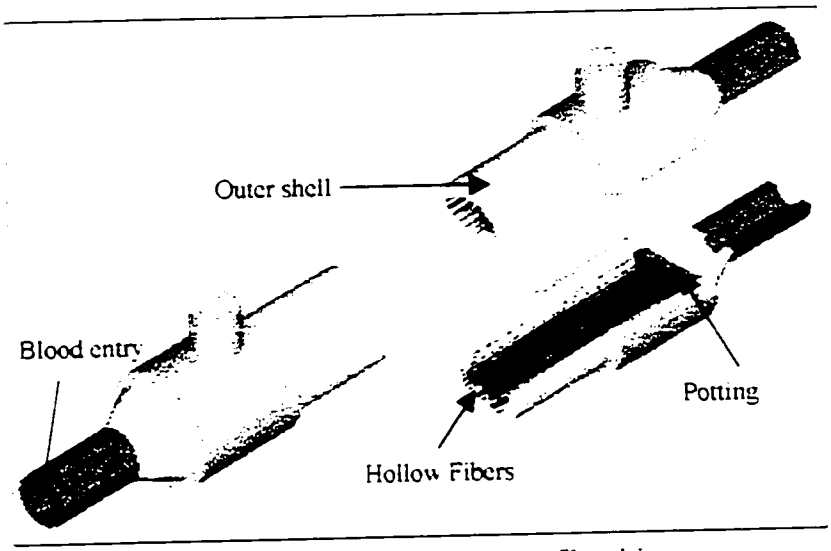

Figure 1.3.1 Diagram of a typical hollow fibre bioreactor

The choice of donor species is an important factor. The candidate must exhibit the following characteristics: (i) it must provide an almost limitless source of islets; (ii) the isolation of the islets must be fairly simple; (iii) the insulin produced by the xenogeneic cells must be similar to human insulin; (iv) the animal's metabolism must be similar to that of humans; and (v) the cells must respond to glucose levels in a manner similar to human pancreatic cells. Pig cells currently exhibit all of these characteristics and are the cells of choice (Bodziony *et al.* 1994, Reach 1993).

Because of its potential as a viable bioartificial pancreas, a great deal of research has been done on the hollow fibre bioartificial pancreas. Different device geometries

have been investigated (Pillarella & Zydney 1990a, Sparks *et al.* 1984, Catapano *et al.* 1990, Pillarella & Zydney 1990b, Moussy & Moussy 1995, Todisco *et al.* 1995, Jaffrin *et al.* 1988). These include the standard device geometry presented above, a U-shaped blood channel and an implantable vascular bioartificial pancreas.

Significant modelling efforts have also yielded interesting results. A number of different models were developed (Pillarella & Zydney 1990a, Catapano *et al.* 1990, Pillarella & Zydney 1990b, Moussy & Moussy 1995, Jaffrin *et al.* 1988, Sparks *et al.* 1982), some of which address the impact of convection and cell distribution on device performance.

One aspect that has not been investigated is the impact of the presence of an osmotically active excluded protein in the ECS. It has been found that the presence of these proteins can reduce convective flow across the membrane (Taylor *et al.* 1994, Taylor & Boukouris 1995, Yeh & Cheng 1994, Patkar *et al.* 1995). This could have an effect on insulin production and delivery. The first half of this thesis presents a model that can predict the impact of convective flow and osmotic effects on device performance.

Another solution to the rejection of xenogeneic islets is to encapsulate them in a semi-permeable microcapsule. As in the hollow fibre, the capsule's pores are sized to exclude all immune factors while permitting exchange of nutrients and insulin. This type of treatment has enormous potential, particularly for chronic diseases such as diabetes.

Most of the research in microencapsulation has dealt with the development of adequate biomaterials. Individual islets are often encapsulated within a hydrophilic alginate gel (Cole *et al.* 1993, Fan *et al.* 1990, Kreslow *et al.* 1991, Levesque *et al.* 1992, Lum *et al.* 1992). A polymer coating can form a size selective membrane with adequate biocompatibility (Mikos *et al.* 1994). Other materials of interest include agarose beads (Dupuy *et al.* 1987), various methacrylates (Stevenson & Sefton 1993), hydrogels (Pathak *et al.* 1992, Doyle *et al.* 1995) and cellulose sulphate (Braun *et al.* 1985).

Microcapsules have an obvious advantage over external hollow fibre devices, but in many ways are also preferable to intravascular implants. Implanted hollow fibres suffer from a high level of thrombosis and generally high cell death rates (Mikos *et al.* 1994). Microcapsules can also be injected intraperitoneally whereas the intravascular device requires a surgical procedure to implant or remove it.

Macrocapsules were also developed but they were quickly found to be inadequate. In a macrocapsule, a large number of islets are contained within a semi-permeable membrane. Mass transfer limitations within the capsules resulted in a lack of nutrients, particularly oxygen, for the cells. As a result, a necrotic core develops in the macrocapsule. The large diffusion length present in macrocapsules also reduced insulin response. Finally the mechanical stability of a large macrocapsule was questionable. The one advantage of the macrocapsule, however, is the possibility to implant and remove it with minimal surgical risk.

1.4 Liver

The liver is commonly known as the body's chemical plant, producing over 600 enzymes (Uchino & Matsushita 1994). The liver's functions include detoxification, protein synthesis and other metabolic processes (Vanholder 1991).

Until recently, whole liver transplantation (often on short notice) has been the only hope for people suffering from liver failure. However, a number of mechanical and bioartificial alternatives are being developed. Although at present none of these can completely replace a patient's native liver for a prolonged period of time, they can provide a bridge to transplantation. By temporarily stabilising a patient's condition prior to surgery, the artificial organ can greatly increase the patient's chances for survival. Further, because of the critical status of many patients awaiting liver transplants, an optimal match between donor and patient is not always possible. An artificial organ would allow more time to find a suitable match between donor and patient, thereby

decreasing the chance of tissue rejection. Given that the source of organs is limited, this becomes a critical issue.

An additional potential benefit of an artificial liver results from the nature of the organ itself. The liver has the capacity to regenerate itself (Malchesky 1994, Lin *et al.* 1979). Currently, this advantage cannot be fully exploited. Fulminant Hepatic Failure (FHF) is a condition that generally requires transplantation (Malchesky 1994, Jauregui & Gann 1991). Although FHF may cause a patient to lose most of his liver, it is a potentially reversible condition. An artificial liver, could keep the patient alive long enough for his or her own liver to regenerate. This in turn would eliminate the need for transplantation.

The liver's ability to regenerate itself also yields an important design advantage. Since FHF is not a chronic problem, there is no requirement to design a small implantable device. A large extra-corporeal device, virtually useless as a long-term solution to diabetes for example, is extremely valuable in the case of liver failure.

Mechanical Devices

A number of purely artificial or mechanical devices have been developed to supplement liver function. Unfortunately the multi-facetted functionality of the liver makes it difficult to replace it with a mechanical device. Hemodialysis with low and high permeability membranes can successfully remove low and middle weight molecular toxins (Shibusawa & Tago 1956, Kiley *et al.* 1956, Schecter *et al.* 1958). Hemofiltration accomplishes the same results. In hemofiltration convection is the primary transport mechanism (Opolon *et al.* 1976), while in hemodialysis diffusive transport dominates. In addition, sorption with coated and uncoated activated carbon has been able to remove high affinity solutes such as organics or protein bound solutes (Malchesky *et al.* 1978).

Some of these techniques are often used in series. For example, sorption can be coupled with hemodialysis or hemofiltration to treat the dialysate or filtrate.

Plasma exchange is another commonly used technique to treat liver failure. All essential plasma products are supplied and the level of toxins is reduced (Agishi *et al.* 1979, Malchesky *et al.* 1980, Nosé *et al.* 1985).

Although the above techniques may help replace some of the native liver's functionality, its metabolic function is either completely ignored or significantly reduced. Bioartificial organs seem to hold greater promise as liver assist device.

Bioartificial Organs

Bioartificial organs will almost certainly prove far more useful than the mechanical devices. When xenogeneic or allogeneic cells are used, all of the liver's functionality can be regained. Most of the development work has centred on the design of an extra-corporeal hollow fibre liver assist device. These devices generally resemble the hollow fibre bioartificial pancreas.

Although different device configurations have been developed, all devices exhibit the same basic characteristics: the cells are separated from the blood stream by a semi-permeable barrier. The cells are therefore immunoisolated and protected from the relatively high shear rates found in the blood (Catapano 1996).

The different configurations that have been developed to optimise device performance can be categorised into two main groups: hepatocytes cultured outside of the hollow fibres and those cultured within the fibre lumens.

The simplest arrangement involving cell culturing in the extra capillary space is virtually identical to the bioartificial pancreas. The cells (individual or in clusters) are either free-floating or bound to microcarriers (Gerlach *et al.* 1993, Knazek *et al.* 1972, Matsura *et al.* 1987, Arnaout *et al.* 1990, Wolf & Munkelt 1975, Hager *et al.* 1978, Rozga *et al.* 1993, Rozga & Holzman 1993). This configuration has the advantage of being versatile as well as quick and easy to seed. Further, commercial membrane

modules can be used (Catapano 1996). Figure 1.4.1 highlights these three configurations. One advantage of the microcarrier bound arrangement is that cryopreservation techniques for this type of cell attachment are quite advanced. Almost 95% of the original viable cells are available after thawing (Catapano 1996).

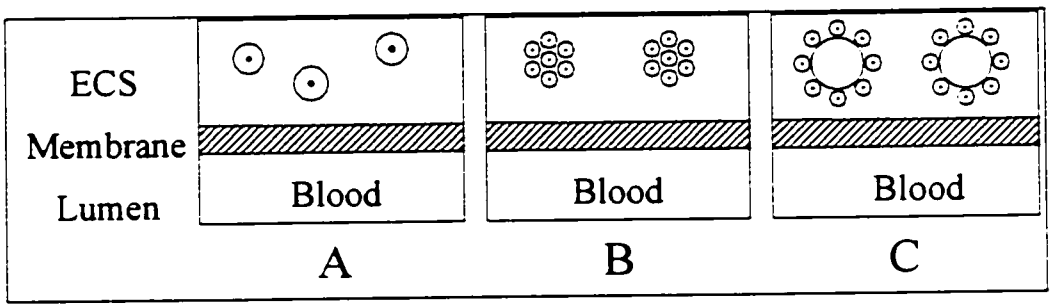

Figure 1.4.1 Three configurations for the suspended cell hollow fibre bioartificial liver. A) individually suspended cells, B) cell clusters, C) microcarrier bound cells (Catapano 1996)

Cell adhesion to a substratum has been proven to promote the long-term maintenance of metabolic function (Gerlach *et al.* 1989). A number of researchers have attempted to develop a device that exploits this characteristic and mimics the native liver's three-dimensional structure. Promising results have been obtained with devices that culture living cells in adhesion outside capillary membranes (Rozga & Holzman 1993, Sussman & Kelly 1993, Neuzil *et al.* 1993, Rozga *et al.* 1994, Sussman *et al.* 1994). This configuration is shown in Figure 1.4.2. After treatment, patients reportedly regained consciousness and the liver tissue appeared to regenerate itself. However, this type of device has two major disadvantages: (i) blood coagulation often required membrane replacement and (ii) necrotic regions developed within the device. The latter problem is related to the additional mass transfer resistance created by the cell mass itself. As a result, deeper cell layers may be devoid of nutrients.

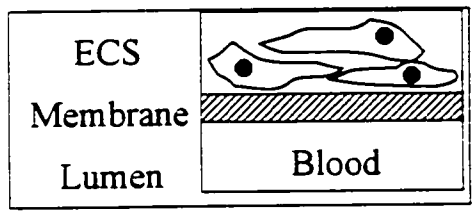

Figure 1.4.2 Hepatocyte layer on the outside of the hollow fibre (Catapano 1996)

Nyberg and colleagues attempted to solve the hepatocyte viability problem with a novel configuration (Shatford *et al.* 1992, Nyberg *et al.* 1992, Nyberg *et al.* 1993, Nyberg *et al.* 1993, Wu *et al.* 1996). The hepatocytes are entrapped and cultured in a collagen gel bed. The bed allows the cells to polarise and differentiate. This generally provides better cell viability than monolayer cultures (Catapano 1996). The gel layer is located in the lumen and blood flows transversely over the exterior of the fibres. Figure 1.4.3 shows an example of this arrangement.

The contraction of the gel normally results in the formation of an unacceptable stagnant layer that hinders mass transport. However, the researchers turned this disadvantage into an advantage; they reduced nutrient depletion by supplying nutrients via intraluminal perfusion.

Blood clotting in this device was also reduced. Since blood flows on the outside of the fibres the number of sharp edges, which is an important factor in the formation of blood clots, is reduced.

A number of problems with this configuration must still be resolved. Nutrient perfusion, this device's strength, is also its Achilles' heel. When perfusion rates are increased, some liver specific factors may be washed out. In addition, the perfusion medium must be sterile and free of endotoxins. This will invariably increase the device's operating cost.

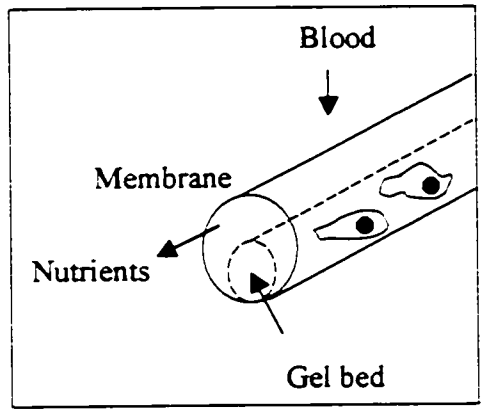

Figure 1.4.3 Collagen entrapped hepatocytes in a hollow fibre (Catapano 1996)

Ironically, the formation of necrotic regions is still a problem. Mass transfer in the gel occurs only by diffusion and large concentration gradients are generally present. Although cell viability has been increased to about one week, a fully functional bioartificial liver that eliminates the need for liver transplant surgery is still to be realised.

Considerable study has been undertaken in the areas of cell cultivation, membrane property optimisation, bioreactor biocompatibility and device geometry. Unfortunately, process modelling has been sorely neglected. Although some mass transfer issues have been addressed, only rudimentary kinetics have been developed and they do not address the issues resulting from the multi-factorial nature of liver insufficiency (Catapano 1996, Giorgio *et al.* 1993, Ohshima *et al.* 1994, Catapano & Bartolo 1996).

The second part of this thesis will therefore be an attempt to extend the model developed for the bioartificial pancreas to the bioartificial liver. The model will be applied to the simplest device geometry where individual cells are suspended in the ECS.

Chapter 2

Model Formulation

2.1 Model Development

Hollow fibre bioreactors have demonstrated great promise as bioartificial organs. This work has therefore centred on these devices.

As mentioned previously, the hollow fibre bioreactor is composed of a bundle of hollow semi-permeable fibres made of polymeric material. These fibres are contained in a plastic shell and potted at both ends. The fluid flowing through the lumen is therefore isolated from the fluid in the extra-capillary space (ECS). A diagram of a typical hollow fibre bioreactor was presented in Figure 1.3.1.

Xenogeneic cells are located in the ECS. The pores in the hollow fibres are sized to exclude immune factors while allowing free passage to nutrients and products. To obtain an adequate pressure drop, the device must be connected as an artero-venous shunt.

Rat beta cells were assumed to populate the bioartificial pancreas while rat hepatocytes were used in the bioartificial liver simulations. Rat cells were chosen because kinetic data was readily available (Pillarella & Zydney 1990a, Ohshima *et al.* 1994, Grodsky 1972).

It is possible to study a multifiber reactor by considering only a single fibre with its associated Krogh cylinder (Patkar *et al.* 1995). Figure 2.1.1 shows a cross sectional representation of a bundle of fibres and their associated Krogh cylinders. The radius of the Krogh cylinder is determined by dividing the total cross sectional surface area of the shell by the number of fibres. No fluid or solute exchange is assumed to occur across a Krogh cylinder boundary as reflected by the symmetry boundary condition that is assumed to exist there. The problem then becomes axisymmetric. This simplification is acceptable in situations where there are no external factors such as poor lumen flow distribution, buoyancy effects or uneven cell distribution in the ECS.

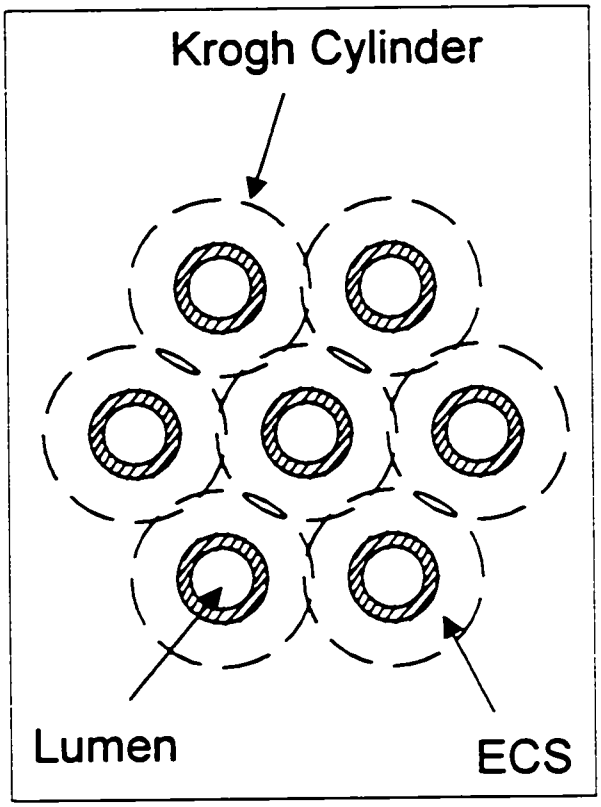

Figure 2.1.1 Krogh cylinder diagram
(Patkar *et al.* 1995)

A diagram of a hollow fibre that includes the co-ordinate system and key geometric parameters is shown in Figure 2.1.2. The fluid enters the fibre at $z = 0$ and exits at $z = L$. The inner radius of the hollow fibre membrane is r_1 while its outer radius is r_2. Meanwhile, the Krogh cylinder boundary is located at r_3.

Because of the porous nature of the membrane and the pressure drop between the inlet and outlet of the lumen, a secondary flow is generated within the extra–capillary space (ECS). In the first half of the fibre, a small portion of the fluid flows from the lumen to the ECS. In the downstream end, the reverse occurs and fluid re–enters the fibre lumen. This phenomenon is known as Starling flow.

As a result of Starling flow, any protein located in the ECS that is too large to penetrate the membrane will have a tendency to accumulate at the downstream end of the

device. This will create an osmotic pressure gradient that will counter Starling flow (Taylor *et al.* 1994). In this analysis, BSA was assumed to be present in the ECS. BSA was chosen because the relationship between BSA concentration and osmotic pressure is well known (Taylor *et al.* 1994, Patkar *et al.* 1995) and because this is a common protein within cell culture media.

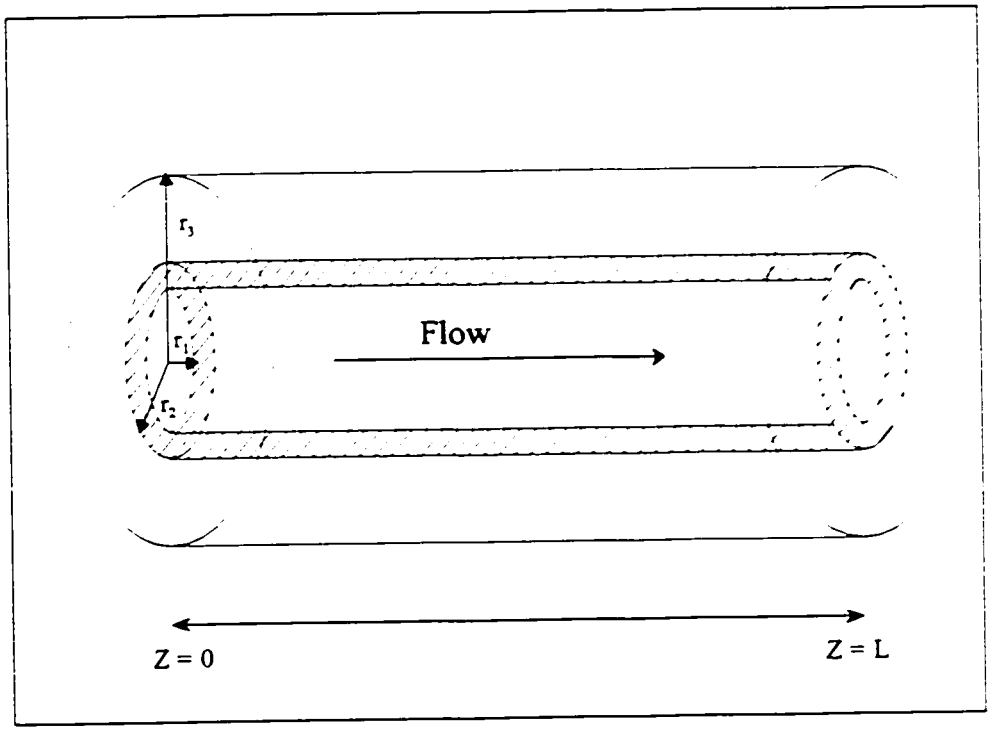

Figure 2.1.2 Diagram of a single fibre (not to scale)

2.2 Hydrodynamics

The hydrodynamics governing HFBR operation have been well documented (Pillarella & Zydney 1990a-b, Jaffrin *et al.* 1988, Taylor *et al.* 1994, Taylor & Boukouris 1995, Yeh & Cheng 1994, Patkar *et al.* 1995, Giorgio *et al.* 1993, Heath *et al.* 1990, Salmon *et al.* 1988, Kelsey *et al.* 1990, Jayaraman 1994, Lemanski & Lipscomb 1995, Labecki *et al.* 1995). A summary of the salient features will be described here; the complete formulation can be found in Taylor *et al.* 1994.

For a constant density, constant viscosity, Newtonian fluid, the momentum and continuity equations can be described as follows:

$$\frac{\partial V}{\partial t} + \mathbf{V} \cdot \nabla \mathbf{V} = -\frac{1}{\rho} \nabla P + \nu \nabla^2 \mathbf{V} \qquad (2.2.1)$$

$$\nabla \cdot \mathbf{V} = 0 \qquad (2.2.2)$$

Although blood is normally considered to be non-Newtonian and better approximated by the Casson model, at shear rates above approximately 100 s^{-1} it becomes essentially Newtonian (Catapano 1996, Tansley 1993). Therefore, as long as the simulations operate above this condition, the fluid can be assumed to be Newtonian. In this study, the simulation with the lowest shear rate had a shear rate of 150 s^{-1}. Because of the rigidity of the fibres and the incompressible nature of the fluid, it can be also assumed that the fluid velocities adjust instantaneously to outside conditions such as changing osmotic pressure conditions in the ECS.

The axisymmetric nature of the hollow fibre allows us to eliminate the above equations' dependency on the θ component. The equations then reduce to a two-dimensional form. The following gives this reduced form for the momentum and continuity equations.

$$\frac{1}{r}\frac{\partial}{\partial r}\left(r\frac{\partial u}{\partial r}\right) = \frac{1}{\mu}\frac{dP}{dz} \qquad (2.2.3)$$

$$\frac{\partial u}{\partial z} + \frac{1}{r}\frac{\partial (rv)}{\partial r} = 0 \qquad (2.2.4)$$

The u and v terms represent the axial and radial velocities respectively. The ordinary differential term found in the momentum equation indicates that the pressure is only a function of the axial position.

The above equations are subject to the following boundary conditions:

$$\frac{\partial u_L}{\partial r} = 0,\ v_L = 0 \text{ at } r = 0 \tag{2.2.5}$$

$$u_L = 0 \text{ at } r = r_1 \tag{2.2.6}$$

$$u_E = 0 \text{ at } r = r_2 \tag{2.2.7}$$

$$\frac{\partial u_E}{\partial r} = 0,\ v_E = 0 \text{ at } r = r_3 \tag{2.2.8}$$

The boundary condition expressed in equation 2.2.5 indicates that there is symmetry at the lumen centreline. The next two equations are no slip boundary conditions, applied at the fluid membrane boundaries. Although it is not exact to assume a no slip condition at the boundary of a porous membrane (Apelblat *et al.* 1974), the low permeabilities found in ultrafiltration membranes justify this simplification. The last boundary condition is the mathematical formulation of the Krogh cylinder symmetry condition.

With the above boundary conditions, it is possible to integrate equations 2.2.3 and 2.2.4 twice with respect to r. These operations yield the axial and radial velocities in the lumen and ECS.

$$u_L(r,z) = -\frac{r_1^2}{4\mu}\frac{dP_L(z)}{dz}\left(1-\frac{r^2}{r_1^2}\right) \tag{2.2.9}$$

$$u_E(r,z) = -\frac{r_2^2}{4\mu}\frac{dP_E(z)}{dz}\left[\frac{2r_3^2}{r_2^2}\ln\left(\frac{r}{r_2}\right)-\left(\frac{r^2}{r_2^2}-1\right)\right] \tag{2.2.10}$$

$$v_L(r,z) = \frac{r_1^3}{16\mu}\frac{d^2P_L(z)}{dz^2}\left(\frac{2r}{r_1} - \frac{r^3}{r_1^3}\right) \tag{2.2.11}$$

$$v_E(r,z) = \frac{1}{16\mu}\frac{d^2P_E(z)}{dz^2}\left[\frac{r_3^4}{r} - r^3 + \frac{2}{r}\left(r_3^2 - r_2^2\right)\left(r_2^2 - r^2\right) - \frac{4r_2^2}{r}\left(r_3^2 \ln\frac{r_2}{r_3} - r^2 \ln\frac{r}{r_2}\right)\right] \tag{2.2.12}$$

With the above equations, it is possible to calculate radially averaged axial velocities:

$$\bar{u}_L(z)\frac{1}{\pi r_1^2}\int_0^{r_1} u_L(r,z)\cdot 2\pi r\,dr \tag{2.2.13}$$

$$\bar{u}_E(z)\frac{1}{\pi\left(r_3^2 - r_2^2\right)}\int_{r_2}^{r_3} u_E(r,z)\cdot 2\pi r\,dr \tag{2.2.14}$$

The equations become independent of the radial co-ordinate. The pressure terms dP / dz found in equations 2.2.9 to 2.2.12 can then be expressed as a function of the radially averaged velocities.

$$\frac{dP_L(z)}{dz} = -\frac{8\mu\bar{u}_L(z)}{r_1^2} \tag{2.2.15}$$

$$\frac{dP_E(z)}{dz} = -\frac{8\mu\bar{u}_E(z)}{\frac{4r_3^4\ln(r_3/r_2)}{r_3^2 - r_2^2} - 3r_3^2 + r_2^2} \tag{2.2.16}$$

Since the velocity equations satisfy continuity, the radially averaged lumen velocity can be directly calculated from the corresponding ECS velocity.

$$\bar{u}_L(z) = \bar{u}_{L0} - \frac{r_3^2 - r_2^2}{r_1^2}\bar{u}_E(z) \qquad (2.2.17)$$

2.3 Membrane Hydrodynamics

Flow through an isotropic relatively impermeable porous membrane can be appropriately calculated by using Darcy's law (Taylor *et al.* 1994). The fluid flux through the membrane is related to the pressure drop across the membrane with the following equation:

$$v_M = -\frac{L_P r_1 \ln(r_2/r_1)}{\mu}\nabla P_M \qquad (2.3.1)$$

The P_M term represents the membrane pressure, L_P is the hydraulic permeability and v_M is the superficial membrane velocity. Because of the very high hydraulic resistance and very low aspect ratios of ultrafiltration membranes, the axial pressure gradients in the lumen and the ECS are much smaller than those found across the membrane. The axial fluid velocity in the membrane is therefore negligible when compared to the radial velocity in the membrane.

When equation 2.3.1 is substituted in the continuity equation, the following ordinary differential equation is obtained.

$$\frac{1}{r}\frac{d}{dr}\left(r\frac{dP_M}{dr}\right) = 0 \qquad (2.3.2)$$

This equation can be integrated from $P_L(z)$ at r_1 to $P_E(z) - \Pi_E(z)$ at r_2 (where the Π term represents the osmotic pressure). When the result of the integration is substituted back into equation 2.3.1, the radial velocity in the membrane is obtained.

$$v_M(r,z) = \frac{L_P}{\mu}\frac{r_1}{r}\left[P_L(z) - P_E(z) + \overline{\Pi}_E(z)\right] \qquad (2.3.3)$$

The osmotic pressure can be related to BSA concentration with a simple virial equation (Patkar *et al.* 1995).

$$\overline{\Pi} = \frac{RT}{M}\left(\overline{C} + A_2\overline{C}^2 + A_3\overline{C}^3\right) \qquad (2.3.4)$$

In the above equation R is the ideal gas constant, T is the absolute temperature, M is the protein molecular weight and A_2 and A_3 are virial constants specific to BSA.

Equations 2.2.15 to 2.2.17 indicate that once the average ECS or lumen velocity is determined, all other hydrodynamic terms can be derived from it. The average ECS velocity can be calculated by performing a fluid balance on an axial ECS element.

$$\frac{d\overline{u}_E}{dz} = \frac{2r_2}{\left(r_3^2 - r_2^2\right)}v_M \qquad (2.3.5)$$

We can substitute the result of equation 2.3.3 into the above equation and eliminate the v_M term.

$$\frac{d\overline{u}_E}{dz} = \frac{2}{\left(r_3^2 - r_2^2\right)}\frac{L_P r_1}{\mu}\left[P_L(z) - P_E(z) + \overline{\Pi}_E(z)\right] \qquad (2.3.6)$$

This equation is not very useful, but if we differentiate it with respect to the z co-ordinate, two dP / dz terms are obtained. Equations 2.2.15 and 2.2.16 can then replace these two terms. This substitution effectively removes the hydrostatic pressure terms.

$$\frac{d^2\overline{u}_E}{dz^2} = \frac{2L_P r_1}{\mu\left(r_3^2 - r_2^2\right)}\left[\frac{8\mu\overline{u}_E(z)}{4r_3^4\left(r_3^2 - r_2^2\right)^{-1}\ln\left(r_3/r_2\right) - 3r_3^2 + r_2^2} - \frac{8\mu\overline{u}_L(z)}{r_1^2} + \frac{d\overline{\Pi}_E(z)}{dz}\frac{d\overline{C}_E}{dz}\right] \tag{2.3.7}$$

Replacing the averaged lumen velocity term with the right side of equation 2.2.17 can eliminate the above equation's dependency on the averaged axial lumen velocity. The final equation is a function of geometric and hydrodynamic parameters, the average ECS axial velocity and the osmotic pressure gradient. Meanwhile, the osmotic pressure gradient is only a function of the local BSA concentration.

$$\frac{d^2\overline{u}_E(z)}{dz^2} - \frac{16L_P\xi}{r_1^3}\overline{u}_E(z) = -\frac{16L_P}{r_1\left(r_3^2 - r_2^2\right)}\overline{u}_{Lo} + \frac{2r_1L_P}{\mu\left(r_3^2 - r_2^2\right)}\frac{d\overline{\Pi}_E}{d\overline{C}_E}\frac{d\overline{C}_E(z)}{dz} \tag{2.3.8}$$

$$\xi = 1 + \frac{r_1^4}{4r_3^4\ln\frac{r_3}{r_2} - \left(r_3^2 - r_2^2\right)\left(3r_3^2 - r_2^2\right)} \tag{2.3.9}$$

2.4 Species Concentration

The standard species conservation equation is required to calculate the concentration of all species present in the lumen and ECS. Previous studies have shown that when radially averaged values are used for the species concentrations, virtually identical results are obtained when compared to those obtained with the more complicated two-dimensional system (Patkar *et al.* 1995). The one dimensional conservation equation is presented below.

$$\frac{\partial\overline{C}_x}{\partial t} = D_x\frac{\partial^2\overline{C}_x}{\partial z^2} - \frac{\partial}{\partial z}\left(\overline{u}_x\overline{C}_x\right) + J_M + Rct \tag{2.4.1}$$

The x subscript in the above equation can be substituted with E or L (corresponding to the ECS or lumen). The D term is the species diffusivity, the J_M term represents the species flux across the membrane and the Rct term is the species reaction (or source) term.

The species conservation equation is subject to the following boundary conditions:

$$\overline{C}_x(t=0) = \overline{C}_{init} \tag{2.4.2}$$

$$\overline{C}_L(z=0) = \overline{C}_0 \tag{2.4.3}$$

$$\frac{\partial \overline{C}_E}{\partial z}(z=0, z=L) = 0 \tag{2.4.4}$$

$$D_L = 0 \tag{2.4.5}$$

The first boundary condition indicates that the initial concentration of all of the species is known. The second one implies that the inlet concentration of all of the species is also known. Since the hollow fibre devices are closed shells, there is no axial outflow of any of the species from the ECS. The third equation mathematically represents this condition. The fourth equation is not actually a boundary condition but its inclusion negates the need for a lumen outflow condition. The high Peclet numbers found in the lumen imply that the downstream species concentrations do not affect the upstream concentrations. By setting the diffusivity in the lumen to zero, no downstream information is required.

The flux term found in equation 2.4.1 is calculated with equations 2.4.6 and 2.4.7 (Klein *et al.* 1979). The flux is based on the outer fibre radius.

$$J_M = \frac{(1-\sigma)v_M}{(1-\exp(-Peclet))}\left(\overline{C}_L - \overline{C}_E \exp(-Peclet)\right)\cdot\frac{2r_2}{\left(r_3^2 - r_2^2\right)} \tag{2.4.6}$$

$$Peclet = \frac{(1-\sigma)v_M}{p_m} \tag{2.4.7}$$

These two equations calculate the contribution of both convective and diffusive transport across the membrane. In the above equations σ is the reflection coefficient and p_m is the species permeability. Since BSA cannot cross the membrane, its reflection coefficient is set to 1. Because of their low molecular size and weight, all of the other species are assumed to freely cross the membrane (Ohshima *et al.* 1994, Klein *et al.* 1979, Fujii *et al.* 1994], hence their reflection coefficients are set to 0.

The source term found in equation 2.4.1 is different for every species. In the case of the bioartificial pancreas, there is only an insulin source term. It is calculated with the following equations.

$$R_{insulin} = \beta_1 \exp[-\alpha_1(t-t_1)] + \beta_2[1-\exp[-\alpha_2(t-t_2)]] \tag{2.4.8}$$

$$\beta_1 = \frac{1.4(C_{glucose} - 0.5)}{3.7 + (C_{glucose} - 0.5)} \tag{2.4.9}$$

$$\beta_2 = \frac{0.59(C_{glucose} - 1.0)}{1.8 + (C_{glucose} - 1.0)} \tag{2.4.10}$$

The above equations describe the biphasic response of the pancreatic beta cells to a glucose challenge (Pillarella & Zydney 1990a, Grodsky 1972). The first compartment (first term of equation 2.4.8) corresponds to an initial quick release of insulin. The contribution from the first compartment quickly tapers off. The second term slowly increases to a maximum value. This maximum value depends on the glucose concentration. The two α terms represent the inverse of the time constants of both compartments and the t_1 and t_2 terms are the compartments' time delays (Pillarella & Zydney 1990a). The following figure highlights this biphasic response following an increase in glucose concentration to 3.0 kg / m^3.

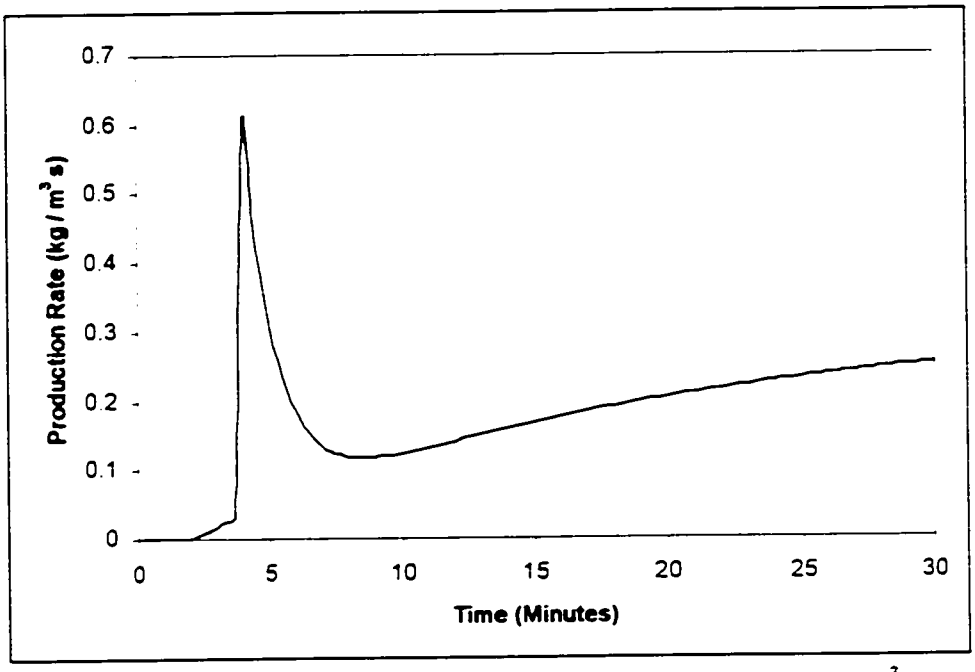

Figure 2.4.1 Insulin production for a glucose challenge of 3.0 kg / m^3

In the case of the bioartificial liver, the two species of concern are ammonia and n-caproic acid (a fatty acid). Both species are consumed by the hepatocytes and require reaction terms. Because of the generally poor viability of hepatocytes in liver assist devices, the reaction rate should also be a function of the viable cell density as well as the species concentration. The cell viability can be calculated with the following first–order equation (Ohshima *et al.* 1994).

$$c = c_{init} \exp(-K_c t) \qquad (2.4.11)$$

The viability is a dimensionless number that ranges from 0 to 1. This number represents the ratio of active hepatocytes to the total number of hepatocytes in the ECS. The K_c term represents the death rate constant while the c_{init} term is the initial hepatocyte viability.

The consumption rate of ammonia and n-caproic acid is a function of the local species concentration as well as the cell density. It is mathematically expressed with the following equation.

$$Rct = -K_x N_0 c \overline{C}_x \qquad (2.4.12)$$

In the above equation, K_x is the metabolic rate constant for ammonia or n-caproic acid while N_0 represents the hepatocyte density. The product N_0c represents the active cell density in the ECS.

Chapter 3

Numerical Procedure

3.1 Species Concentration

The species concentration equation (2.4.1) must be solved in order to determine the concentration of all of the relevant species in the ECS and lumen. Since this partial differential equation cannot be solved analytically, a control volume method developed by Patankar was used (Patankar 1980). A summary of this numerical procedure will now be presented.

Patankar's control volume method requires the discretization of the continuum into a set of non-overlapping sub units or control volumes. The differential equation is then integrated over each control volume by assuming a profile for the dependent variables. This yields a set of algebraic equations that can be solved using standard techniques. The dependent variables are therefore approximated by piece wise profiles and the resultant algebraic equations express the conservation principle for the finite control volumes, just as the differential equation expresses it for infinitesimal control volumes.

A diagram of a typical control volume is presented in Figure 3.1.1. The species concentration is represented with the variable ϕ. The central node is labelled ϕ_P while the eastern and western nodes are ϕ_E and ϕ_W respectively. The concentration is calculated only at each node.

The e and w faces bound the central control volume. The width of the control volume is denoted by Δx. The other Δx terms represent the distance between the nodes and their control volume boundaries. Although the diagram seems to indicate that all nodes are equally spaced, this is not a requirement of the method.

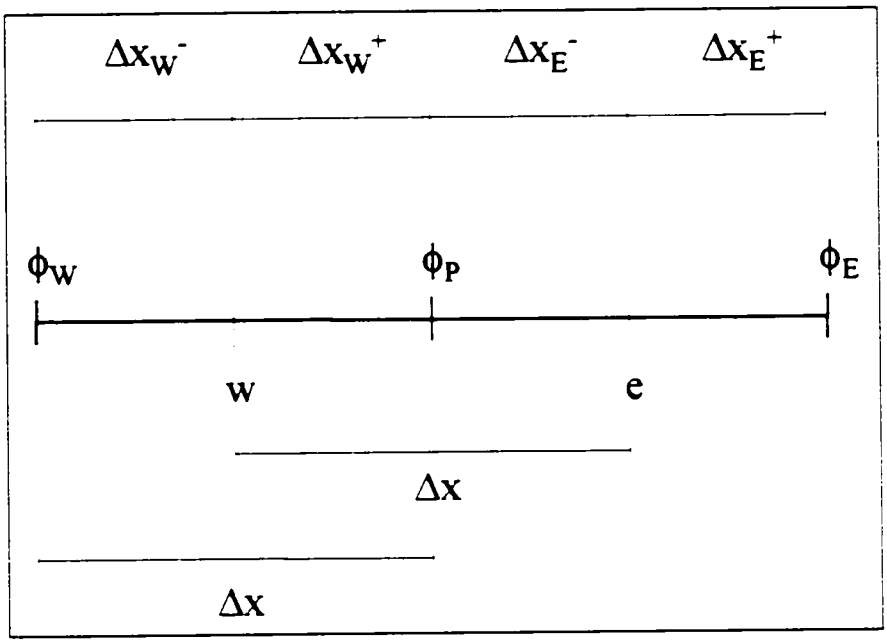

Figure 3.1.1 Control volume diagram

The development of the control volume method is quite involved and outside the scope of this thesis. Instead, the final form of the equation for node P is presented below.

$$a_P\phi_P = a_E\phi_E + a_W\phi_W + b + F_e - F_w \tag{3.1.1}$$

The coefficients a_P, a_E, a_W and b are defined in the following equations.

$$a_E = \Gamma_e A(|Peclet_e|) + \max[-F_e, 0] \tag{3.1.2}$$

$$a_W = \Gamma_w A(|Peclet_w|) + \max[F_w, 0] \tag{3.1.3}$$

$$b = S_C\Delta x + a_P^0\phi_P^0 \tag{3.1.4}$$

$$a_P^0 = \frac{\Delta x}{\Delta t} \tag{3.1.5}$$

$$a_P = a_E + a_W + a_P^0 - S_P \Delta x \tag{3.1.6}$$

$$F_e = \bar{u}_e \tag{3.1.7}$$

$$F_w = \bar{u}_w \tag{3.1.8}$$

$$\Gamma_e = \frac{D_e}{\Delta x_E^- + \Delta x_E^-} \tag{3.1.9}$$

$$\Gamma_w = \frac{D_w}{\Delta x_W^- + \Delta x_W^-} \tag{3.1.10}$$

$$Peclet_e = \frac{F_e}{\Gamma_e} \tag{3.1.11}$$

$$Peclet_w = \frac{F_w}{\Gamma_w} \tag{3.1.12}$$

$$A(|Peclet|) = \max\left\{0, (1 - 0.1|Peclet|)^5\right\} \tag{3.1.13}$$

In the above equations, the F terms represent convection, the Γ terms represent diffusion, the u terms are the fluid velocities, the D terms are the diffusivities and S_C and S_P are source terms.

Equation 3.1.1 is essentially the conservation equation for one control volume. The concentration value at node P at time t is influenced by the concentration at the adjacent nodes, by the concentration at node P at the previous time step and by the presence of a source or sink term.

The a_E and a_W coefficients measure the impact that the east and west nodes have on the central node's final value. The Γ terms represent species diffusive flux across the eastern and western boundaries. The F terms, meanwhile, represent the species convective flux across these same boundaries. The impact of both modes of mass transfer is calculated by using the function in equation 3.1.13. This function, commonly known as the power law, uses the absolute value of the Peclet number to determine the relative contribution of convective and diffusive mass transfer. Most standard finite difference algorithms use a linear approximating function for the dependent variable ϕ to calculate the flux at the control volume faces. This is known as the central difference approximation. Patankar demonstrated that for situations where a high degree of convection is present, this approximation yields physically unrealistic values for the dependent variable. For these situations an upwinding technique is required. When there is a high degree of convection, the value of ϕ at the control volume boundary will be closer to the value of ϕ at the node that is upstream (or upwind) of it. An upwind scheme will properly incorporate this effect.

The power law is an upwinding technique. However, unlike many other upwinding techniques, the power law properly calculates the fluxes when the Peclet number is low. If, for example, the Peclet number is 0, a_W and a_E equal the diffusion terms Γ_w and Γ_e, respectively. At low Peclet numbers, the power law and central difference schemes yield virtually identical results. Conversely, when the Peclet number is large and positive, a_W becomes equal to F_w and a_E reduces to 0. For a large and negative Peclet number, the terms are reversed: a_W reduces to 0 and a_E equals F_e.

In the control volume method, the reaction term (or source term) is represented by the variables S_C and S_P. This method requires that the source term be a linear function; hence, if the source term is non-linear, it must be linearised by performing a Taylor series expansion. In the following equation, the S_C term represents the ϕ independent portion of the equation while the S_P term represents the ϕ dependent portion of the equation.

$$S(\phi) = S_C + S_P\phi \qquad (3.1.14)$$

Another prerequisite for this method is that the S_P term be negative or 0. Patankar has demonstrated that for the system to yield physically realistic results the coefficients a_W, a_E and a_P must be all positive. If S_P were positive, equation 3.1.6 could yield a negative a_P which, in turn, could lead to physically meaningless results (in this case, negative concentrations).

As mentioned previously, the source term sometimes needs to be linearised. This can be accomplished by taking the equation's Taylor series expansion and dropping all terms of second–order or greater. Since the linear equation only approximates the actual source term, iterations are generally required to obtain an accurate solution. The following equation is the source term's Taylor series expansion. The expansion is performed around ϕ^*, the previous iteration's ϕ value.

$$S(\phi) = S^* + \left(\frac{dS}{d\phi}\right)^* \left(\phi_P - \phi_P^*\right) \qquad (3.1.15)$$

The solution to the previous equations is not bound to any particular algorithm. The tri-diagonal-matrix-algorithm (TDMA) has proved itself quite useful as a control volume method solver (Patankar 1980). If we rename the nodes ϕ_P, ϕ_E and ϕ_W to ϕ_i, ϕ_{i-1} and ϕ_{i-1}, the discretization equation for node i becomes,

$$a_{P_i}\phi_i = a_{E_i}\phi_{i-1} + a_{W_i}\phi_{i-1} + b_i \qquad (3.1.16)$$

where b_i represents all source and ϕ independent terms.

If the leftmost node is node 1 and the last node is node N, nodes 0 and N+1 play no meaningful role. This essentially means that a_{W1} and a_{EN} can be set to 0. Node 1 can

therefore be expressed as a function of node 2 and by extension, ϕ_i can be expressed as a function of ϕ_{i-1}. The following equations summarise the rearrangement.

$$\phi_i = B_i \phi_{i-1} + Q_i \tag{3.1.17}$$

$$B_i = \frac{a_{Ei}}{a_{Pi} - a_{Wi} B_{i-1}} \tag{3.1.18}$$

$$Q_i = \frac{b_i + a_{Wi} Q_{i-1}}{a_{Pi} - a_{Wi} B_{i-1}} \tag{3.1.19}$$

The boundary conditions can then be incorporated into equations 3.1.18 and 3.1.19 for nodes 1 and N. In the case of node 1 the values for B and Q are the following:

$$B_1 = \frac{a_{E1}}{a_{P1}} \tag{3.1.20}$$

$$Q_1 = \frac{b_1}{a_{P1}} \tag{3.1.21}$$

If the value of ϕ_1 is known, this boundary condition can be incorporated by setting a_{E1} to 0, a_{P1} to 1 and b_1 to the value of ϕ at the boundary. If the flux is known, its value is independent of ϕ. The flux is therefore directly included in the b_1 term. For either situation, B_1 and Q_1 can be calculated.

A similar technique can be used to incorporate the eastern boundary condition. As mentioned previously, a_{EN} is set to 0. Since a_{EN} is 0, P_N is also 0. If the value of ϕ_N is known, Q_N can be set to ϕ_N. Conversely, if the flux is known, its value is once again incorporated into the b term. Q_N can then be calculated with equation 3.1.19.

By solving the control volume equations with the TDMA algorithm, the concentration of all species in the lumen and ECS can be calculated. In the bioartificial pancreas, the concentration of glucose and insulin in the ECS and lumen is determined. In the bioartificial liver, the concentration of ammonia and n-caproic acid in the lumen and ECS is calculated. For both systems, the ECS BSA concentration is also determined. (Only the ECS concentration is required because BSA is excluded from the membrane.)

3.2 Hydrodynamics

The second–order differential equation represented by Equation 2.3.8 is the main hydrodynamic equation. The presence of an osmotic pressure term complicates the situation since the solution of the hydrodynamic equation requires the local BSA concentration.

The coupling of the hydrodynamic equation and the BSA conservation equation would normally require an iterative solution. The BSA concentration would be calculated using an assumed velocity and a revised velocity field could then be calculated with the newly obtained BSA concentration profile. The BSA could then be recalculated with the new velocity values. This process would continue until convergence was achieved.

Because the iteration must be performed at every time step, the coupling of these two equations would considerably slow down the calculations. However, since protein polarisation is a slow process compared to fluid residence time in the hollow fibre device, the fluid velocity between two time steps will not differ greatly provided the time steps are sufficiently small. By lagging the velocity calculations by one time step, the two equations are effectively uncoupled and can be solved independently for a single time step.

Since velocity calculations are now lagged by one time step, equation 2.3.8 becomes a linear second order differential equation. This type of equation can be solved

with a simple fourth–order Runge-Kutta algorithm. The second–order equation can be transformed into two first–order equations by employing a substitution variable (Press *et al.* 1992).

$$\frac{d^2u}{dz^2} + q(z)\frac{du}{dz} = m(z) \tag{3.2.1}$$

$$\frac{du}{dz} = n(z) \tag{3.2.2}$$

$$\frac{dn}{dz} = m(z) - q(z)n(z) \tag{3.2.3}$$

The above equations require two boundary conditions: u(0) and n(0). Unfortunately the boundary conditions for this particular problem are located at both ends of the ECS. In the above three equations, this is equivalent to knowing u(0) and u(L). A shooting technique is therefore required to solve the hydrodynamic equation (Kincaid & Cheney 1991).

The shooting technique is essentially a trial and error solution. The unknown initial conditions are assumed and the system of equations is solved. The solution at the end point is then compared to the boundary condition value. The initial guess is corrected and the process is repeated. Figure 3.2.1 graphically highlights the shooting procedure.

One of the advantages of a linear system of equations is that the exact solution can be calculated directly from a linear combination of two guesses. Two different values are assumed for the initial velocity gradient (du / dz) and the solutions are then calculated. The following equations highlight this procedure.

$$\begin{aligned} u_1(0) &= u_0 \qquad n_1(0) = \alpha \\ u_2(0) &= u_0 \qquad n_2(0) = \beta \end{aligned} \tag{3.2.4}$$

$$u(z) = \lambda u_1(z) + (1-\lambda) u_2(z) \tag{3.2.5}$$

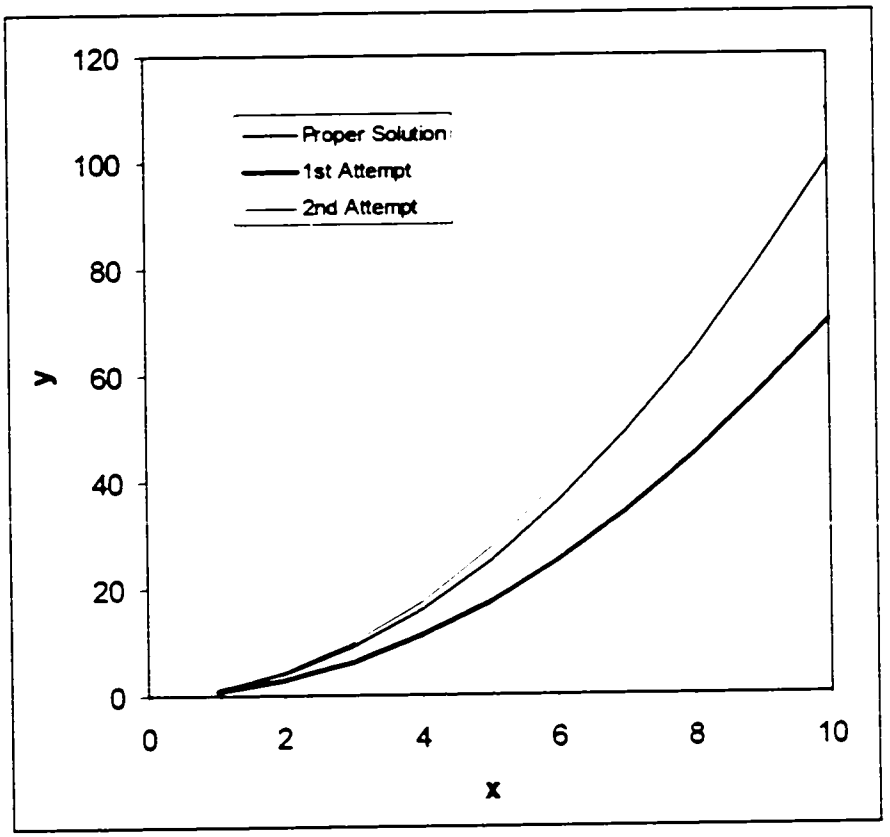

Figure 3.2.1 Shooting method diagram

The terms α and β can be any two distinct values. The simplest approach is to assign the value α + 1 to β. In equation 3.2.5, λ is a weighting factor that is extracted from the boundary condition u(L).

$$\lambda = \frac{u(L) - u_2(L)}{u_1(L) - u_2(L)} \tag{3.2.6}$$

3.3 BSA Concentration Gradient

The procedure outlined in section 3.2 yields the axial fluid velocity at every node and control volume face. Unfortunately, the concentration and concentration gradient required in equation 2.3.8 are obtained from a grid that is half as dense as the velocity grid. These values must therefore be interpolated from the discrete set of BSA concentration values obtained with the procedure outlined in section 3.1. This can be accomplished with a cubic spline (Kincaid & Cheney 1991). A cubic spline was chosen because it guarantees a continuity of slope and curvature at the spline boundaries. The cubic spline, which is essentially a series of cubic polynomials, can be represented by the following equation:

$$S_i(x) = a_i + b_i x + c_i x^2 + d_i x^3 \tag{3.3.1}$$

The above equation has four unknown coefficients. Assuming that we have N+1 points located at points x_0, x_1 ... x_N with concentration values of y_0, y_1 ... y_N, intermediate points can be approximated with N cubic polynomials. Equation 3.3.2 shows that each equation is applied to a different region. There are therefore 4N unknown coefficients.

$$S(x) = \begin{cases} S_0(x) & x \in [x_0, x_1] \\ S_1(x) & x \in [x_1, x_2] \\ \vdots & \vdots \\ S_{N-1}(x) & x \in [x_{N-1}, x_N] \end{cases} \tag{3.3.2}$$

Since the y values at spline boundaries are given, we know that $S_i(x_i) = y_i$ and $S_i(x_{i-1}) = y_{i-1}$. This reduces the number of unknowns by 2N. By incorporating the continuity of slope and curvature at the spline boundaries, the number of unknowns is further reduced by 2(N-1). Only two degrees of freedom remain and they can be determined by setting boundary conditions at x_0 and x_N. These boundary conditions were

listed in Equation 2.4.4. There is no axial outflow at the boundaries. These first derivatives are therefore 0.

After making all of the necessary substitutions, the final form of the cubic polynomial is obtained.

$$S_i(x) = y_i + (x - x_i)[C_i + (x - x_i)[B_i + (x - x_i)A_i]] \tag{3.3.3}$$

$$A_i = \frac{1}{6h_i}(z_{i-1} - z_i) \tag{3.3.4}$$

$$B_i = \frac{z_i}{2} \tag{3.3.5}$$

$$C_i = -\frac{h_i}{6}z_{i-1} - \frac{h_i}{3}z_i + \frac{1}{h_i}(y_{i-1} - y_i) \tag{3.3.6}$$

$$h_i = x_{i-1} - x_i \tag{3.3.7}$$

In the above equations, the term z_i represents the first derivative of the cubic spline. The z_i terms for splines 1 to N-1 can be calculated by solving the following matrix.

$$\begin{bmatrix} u_1 & h_1 & & & & & \\ h_1 & u_2 & h_2 & & & & \\ & h_2 & u_3 & h_3 & & & \\ & & \ddots & \ddots & \ddots & & \\ & & & h_{N-3} & u_{N-2} & h_{N-2} & \\ & & & & h_{N-2} & u_{N-1} & \end{bmatrix} \begin{bmatrix} z_1 \\ z_2 \\ z_3 \\ \vdots \\ z_{N-2} \\ z_{N-1} \end{bmatrix} = \begin{bmatrix} v_1 \\ v_2 \\ v_3 \\ \vdots \\ v_{N-2} \\ v_{N-1} \end{bmatrix} \tag{3.3.8}$$

$$u_i = 2(h_i + h_{i-1}) \tag{3.3.9}$$

$$b_i = \frac{6}{h_i}(y_{i-1} - y_i) \tag{3.3.10}$$

$$v_i = b_i - b_{i-1} \tag{3.3.11}$$

The terms z_0 and z_N, meanwhile, are already known from boundary condition 2.4.4. Since dC / dz = 0 at the boundaries, z_0 and z_N are also 0.

3.4 Computer Program

The program used to solve the system of equations was written in C++ using Microsoft's Visual C++ compiler version 4.0. The program's validity was assured by comparing the numerical solutions of simpler problems to their analytical solutions. The results of these tests are presented in Appendix 1. The simulations were performed on a 166-megahertz Intel Pentium machine running Microsoft's Windows NT version 4.0.

Chapter 4

Results and Discussion

4.1 Simulation Objectives

As mentioned previously, the purpose of this thesis was to investigate the effect of hollow fibre bioreactor hydrodynamics on the performance of a bioartificial pancreas and liver. In addition to nutrients supplied from the blood, cells generally require various growth factors when cultured in bioartificial systems. Cell culture media often contain buffers (HEPES and Krebs), saline solutions, calf serum, hydrocortisone, antibiotics and bovine serum albumin (BSA) (Catapano *et al.* 1990, Todisco *et al.* 1995, Wolf & Munkelt 1975, Hager *et al.* 1978, Shatford *et al.* 1992, Nyberg *et al.* 1992, Aung *et al.* 1993, Ramirez *et al.* 1992). It has been found that the polarisation of a high molecular weight protein such as BSA, which is isolated in the ECS by the hollow fibre membrane, can reduce convective transport across the membrane (Taylor *et al.* 1994, Taylor & Boukouris 1995, Patkar *et al.* 1995, Labecki *et al.* 1995). This reduction may hinder device performance. Since the relationship between BSA concentration and the osmotic pressure is known, a parametric study based on BSA concentration in the ECS was performed.

Many different types of ultrafiltration membranes are available. Bioartificial organs that use polysulfone, (Pillarella & Zydney 1990a, Wolf & Munkelt 1975, Nyberg *et al.* 1992, Nyberg *et al.* 1975), polyamide (Catapano *et al.* 1990, Todisco *et al.* 1995, Ohshima *et al.* 1994), cellulose nitrate / cellulose acetate (Rozga *et al.* 1993a) and polyethylene (Takeshita *et al.* 1995) have been developed. These membranes have different properties relating to mass transfer and hydrodynamics such as species permeability and hydraulic permeability that may vary greatly among membranes. For this reason, the simulations were also conducted under different mass transfer regimes. The species permeability was varied to yield two systems. In the first system, convection was the primary mass transfer mechanism. In the second system, diffusion was the most important mass transfer mechanism.

Although many papers have been published concerning the performance of bioartificial devices, most of these results involve the survivability of animals connected

to bioartificial organs (Rozga *et al.* 1993a-b, Rozga *et al.* 1994, Sussman *et al.* 1992, Ohzato *et al.* 1992, Bodziony 1992). The available data that could provide a comparison between these simulations and experimental results is expressed in a form that makes it difficult to yield direct comparisons. As a result, only model simulations are presented here.

4.2 Pancreas

Two sets of bioartificial pancreas simulations were performed. The first set of simulations were performed at a glucose and insulin permeability of 1.625×10^{-7} m / s and 3.625×10^{-8} m / s respectively. In the second set, these values were increased to 2.6×10^{-6} m / s and 5.8×10^{-7} m / s. In each set, simulations were performed for a range of initial BSA concentrations: 0 kg / m^3, 5 kg / m^3 and 50 kg / m^3. The species permeabilities were varied to investigate the importance of polarisation on devices where convection is the dominant trans–membrane mass transfer mechanism as well as those where diffusion is the dominant transport mechanism across the hollow fibre wall.

Table 4.2.1 summarises the parameters common to all simulations. The geometric, hydrodynamic and reaction rate parameters were taken from Pillarella & Zydney 1990a. The reaction rate terms α_1, α_2, t_1 and t_2 depend greatly on the initial and inlet glucose concentrations and on the geometric parameters. The parameters in these simulations therefore needed, as much as possible, to match those found in Pillarella & Zydney 1990a. The osmotic pressure relationship and the virial coefficients were taken from Patkar *et al.* 1995.

Low Membrane Permeability

The first set of pancreas simulations was performed at low species permeabilities. The device performance can be gauged by measuring the total insulin exiting the lumen. This value at any given time can be obtained by multiplying the lumen outlet insulin concentration by the fluid velocity and the lumen cross sectional area. This is

represented in equation 4.2.1. The total cumulative insulin output can be calculated with equation 4.2.2.

Table 4.2.1: Parameters common to all pancreas simulations (Pillarella & Zydney 1990a, Patkar *et al.* 1995)

Parameter	Value
Glucose diffusivity in the ECS (m^2 / s)	9.1×10^{-10}
Insulin diffusivity in the ECS (m^2 / s)	2×10^{-10}
Glucose diffusivity in the lumen (m^2 / s)	0
Insulin diffusivity in the lumen (m^2 / s)	0
BSA diffusivity (m^2 / s)	1×10^{-10}
Initial ECS glucose concentration (kg / m^3)	1
Initial lumen glucose concentration (kg / m^3)	1
Inlet glucose concentration (kg / m^3)	3
Initial ECS insulin concentration (kg / m^3)	0
Initial lumen insulin concentration (kg / m^3)	0
Inlet insulin concentration (kg / m^3)	0
Fibre length (m)	0.15
Inner fibre radius (μm)	500
Outer fibre radius (μm)	670
Krogh cylinder radius (μm)	1400
Hydraulic permeability (m)	2.9×10^{-12}
Inlet Velocity (cm / s)	74.91
BSA molecular weight (g / mol)	69000
Viscosity (Pa s)	0.000694
First osmotic virial coefficient A_2 (m^3 / kg)	10.473×10^{-3}
Second osmotic virial coefficient A_3 (m^6 / kg^2)	17.374×10^{-6}
Temperature (°K)	310
First time constant - α_1 (1 / s)	0.013
Second time constant - α_2 (1 / s)	0.001
First time delay - t_1 (s)	240
Second time delay t_2 (s)	120
Time step (s)	0.2
Number of control volumes	200
Simulation duration (hours)	5

$$\dot{m}_{insulin}(t) = \pi r_1^2 \bar{u}_L(L,t)\bar{C}_{Linsulin}(L,t) \qquad (4.2.1)$$

$$\sum_{t=0}^{t} \dot{m}_{insulin}(t)\Delta t \qquad (4.2.2)$$

Figure 4.2.1 shows that the presence of BSA in the ECS greatly impaired device performance. In considering these results, it is noted that a low insulin output rate can be caused by two phenomena: reduced insulin production and reduced insulin membrane flux. The influence of these two factors in the insulin production rates shown in Figure 4.2.1 will now be addressed.

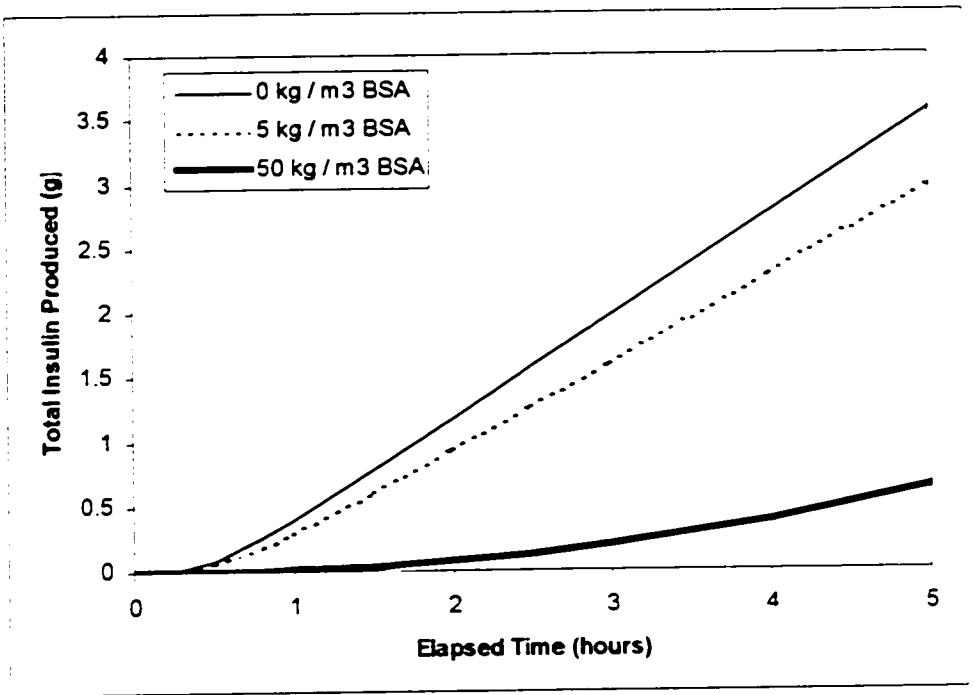

Figure 4.2.1 Total insulin produced by the low species permeability systems

Insulin is produced in response to a glucose challenge. If more glucose penetrates the ECS, more insulin will be produced. Figure 4.2.2 shows the average ECS glucose concentration as a function of time. This figure clearly indicates that, when no protein is present, the average ECS glucose concentration reaches its maximum value of 3 kg / m^3 after about one hour of operation. When 50 kg / m^3 of BSA is present, over five hours are required to attain this level. The additional glucose in the first simulation will

therefore generate more insulin. The reason for this quicker exchange of glucose to the ECS will be explained later.

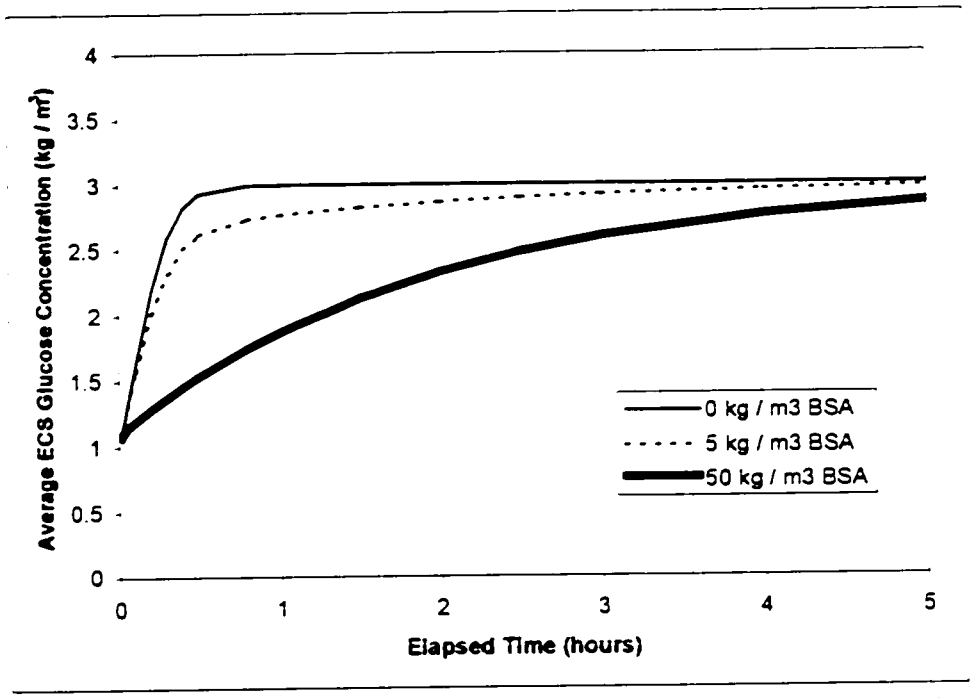

Figure 4.2.2 Average ECS glucose concentration for the low permeability systems

The average insulin flux across the membrane is plotted as a function of time in Figure 4.2.3. This figure shows that the flux term when no protein was present is much greater than that observed when 50 kg / m^3 was present. (The actual insulin flux values are negative since they represent a flux from the ECS to the lumen. The signs were reversed to simplify the figure.) The higher flux values observed when no protein was present are not only caused by the higher insulin production rate but also by the higher insulin mass transfer rate. Even though the average glucose concentration in the first simulation was at most twice as high as that observed in the third simulation, the insulin flux was always at least three times higher. This indicates that, in addition to a higher insulin generation term, insulin mass transfer across the membrane must also be higher when no protein is present.

The above observation is confirmed by Figure 4.2.4. Even though less insulin was produced when 50 kg / m^3 of BSA was located in the ECS, the insulin concentration was much higher than when no ECS protein was present. In the absence of protein, the insulin that is produced quickly re-enters the lumen by convection and exits the device. Furthermore, as will be shown later, the regions where the insulin concentration was highest correspond to regions where convective transport was eliminated.

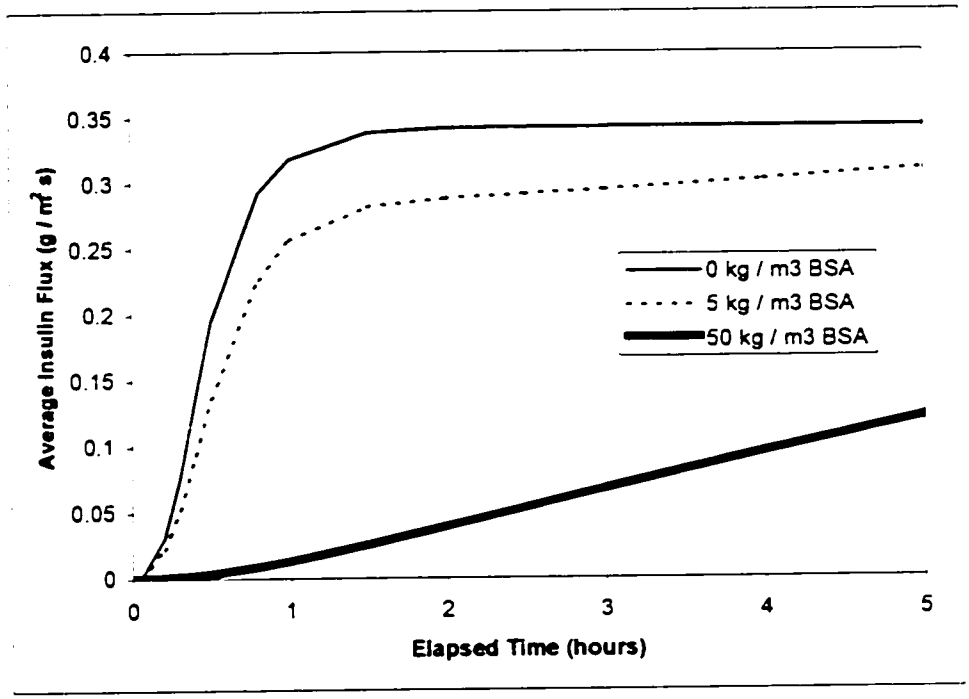

Figure 4.2.3 Average insulin flux for the low species permeability systems

The insulin profiles in the device after five hours of operation are plotted in Figure 4.2.5. These profiles were established after half an hour of operation. Aside from an initial transitory period where glucose begins to accumulate in the ECS and insulin production begins, the relative shape of the profiles shown in Figure 4.2.5 are representative of those found at any other time in the device.

When no protein was present, the insulin flux in the downstream end of the device was much greater than that obtained when 50 kg / m^3 of BSA was present. Meanwhile,

the flux in the upstream end of the device was slightly greater with an initial BSA concentration of 50 kg / m^3 when compared to the case where no protein was present.

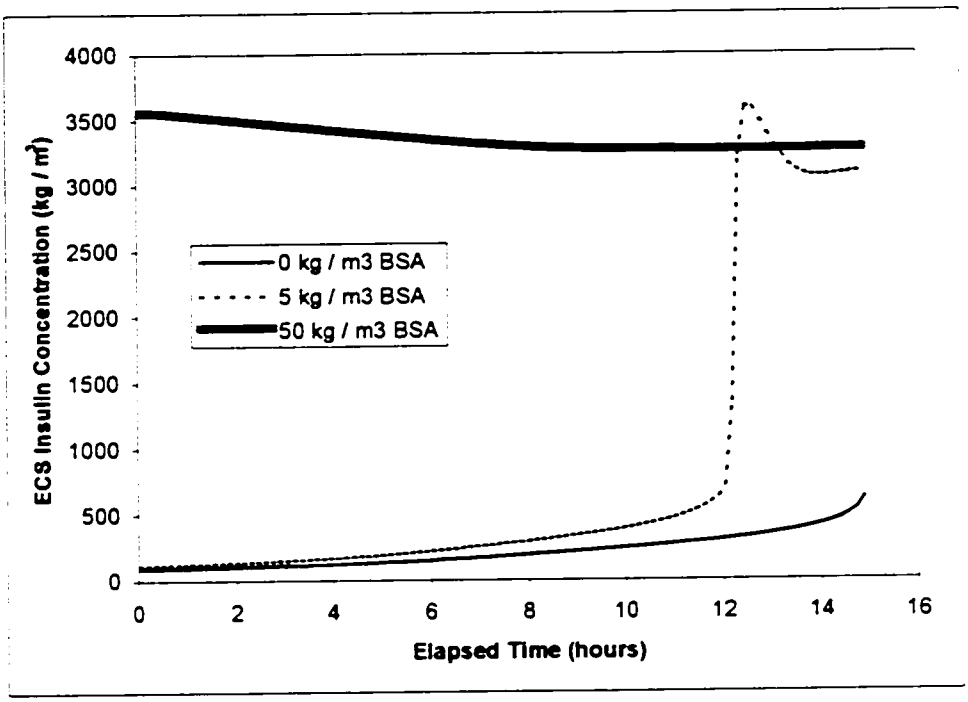

Figure 4.2.4 Insulin concentration profile after five hours of operation for the low species permeability systems

The profiles obtained in Figures 4.2.1 to 4.2.5 can be understood by examining the fluid flux profiles found in Figure 4.2.6. The fluid flux obtained when no protein was present is representative of pure Starling flow. In the upper half of the device, there is a net flow of fluid from the lumen to the ECS. In the downstream end, the reverse is observed. This positive flux in the first half of the device will increase the speed of glucose delivery while the negative flux in the downstream end of the device will enhance the rate at which insulin is extracted from the ECS.

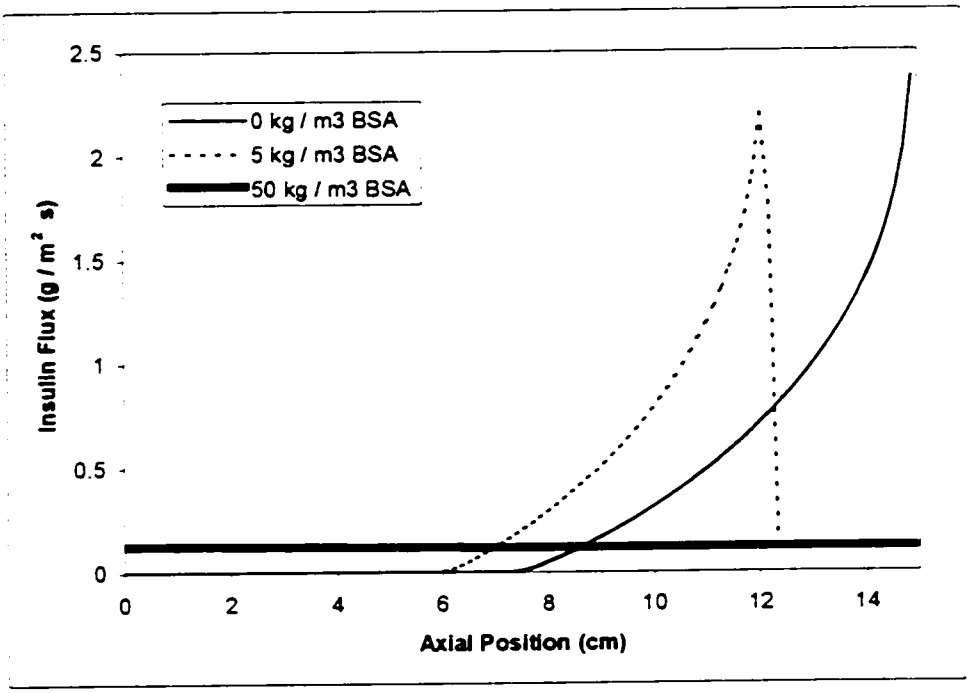

Figure 4.2.5 Insulin flux after 5 hours of operation for the low species permeability systems

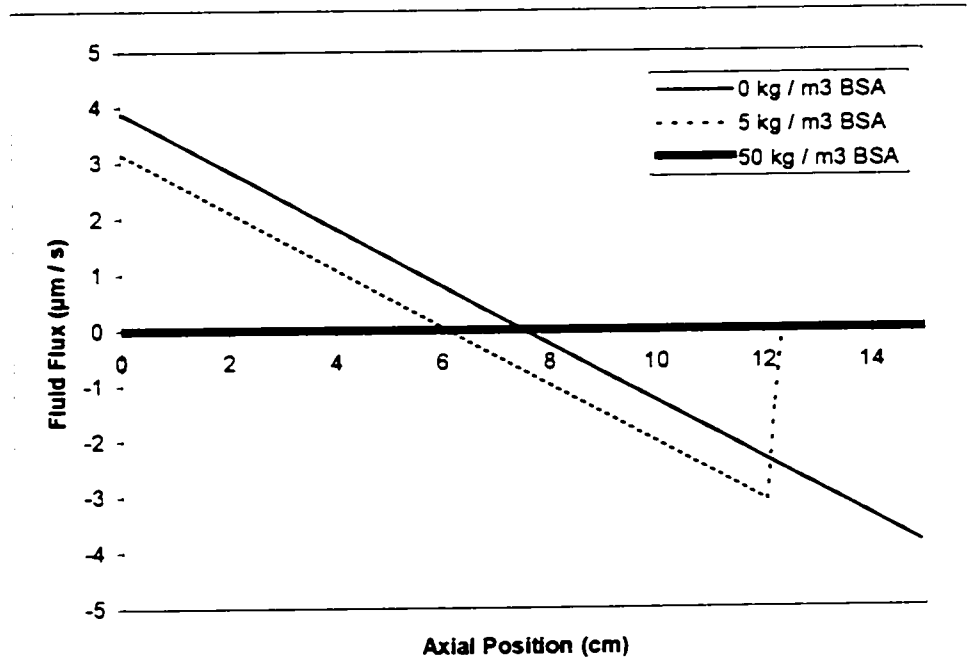

Figure 4.2.6 Fluid flux profiles for the low species permeability systems after 5 hours of operation

When an excluded protein such as BSA is present, it accumulates in the downstream end of the device. This can be seen in Figure 4.2.7. This polarisation causes an osmotic pressure gradient that counteracts the pressure gradient responsible for Starling flow. This reduces flow across the membrane (see Figure 4.2.6) and therefore also reduces the convective transport of glucose and insulin across the membrane.

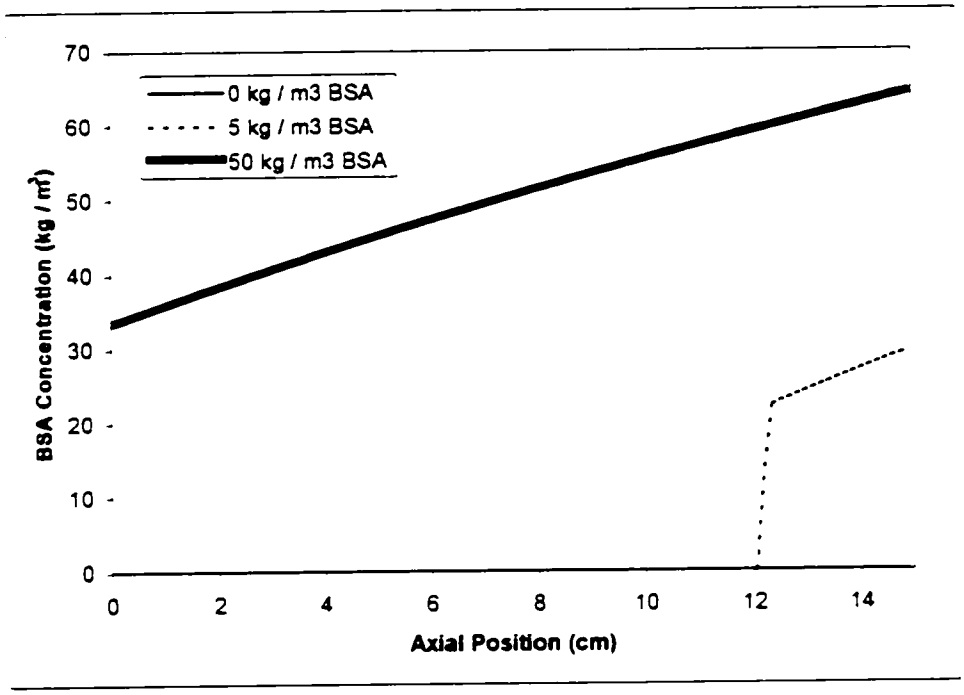

Figure 4.2.7 BSA Concentration profiles for low species permeability systems after 5 hours of operation

The reduction in fluid exchange becomes more dramatic as the amount of protein loading in the device increases. In fact, when 50 kg / m^3 of BSA is initially present in the ECS, mass transfer across the membrane essentially occurs only by diffusion. (Note that a small amount of convection is always present to sustain the protein gradient in the ECS.) This virtual elimination of trans–membrane convection happens quickly: the fluid flux is reduced by two orders of magnitude after 12 minutes of operation with a BSA loading of 50 kg / m^3.

The elimination of convection also explains the presence of a small insulin flux to the lumen in the upstream half of the device at this same protein loading. Normally, convection from the lumen to the ECS precludes transport of insulin from the ECS in this region of the device. On the other hand, when convection is eliminated, insulin can diffuse from the ECS to the lumen. However, this slight advantage in insulin uptake from the upstream end of the device does not offset the huge reduction in insulin transport observed at the downstream end.

High Membrane Permeability

The previous set of simulations demonstrated that protein polarisation had a significant impact on device performance when convection was the predominant mass transfer mechanism. In the second set of simulations, the impact of polarisation on the performance of a device that uses diffusion as a primary mass transfer mechanism was investigated.

In this second group of simulations, the glucose and insulin permeabilities were raised to 2.6×10^{-6} and 5.8×10^{-7} m / s. All other parameters were identical to those of the previous group of simulations. The species permeabilities were chosen to isolate the effects to the diffusion of glucose and insulin across the membrane. As a consequence, the total amount of fluid that crosses the membrane boundary is identical to that of the first set of simulations. Furthermore, protein polarisation is independent of glucose and insulin permeability. As a consequence the fluid flux and BSA concentration profiles obtained in this set of simulations are identical to those of the first group.

Figure 4.2.8 shows the total insulin produced as a function of time for the three simulations in this set. From this figure, we see that the impact of polarisation on device performance is negligible when compared to that in the first set of simulations. When 5 kg / m^3 of BSA is initially present, the insulin output after five hours of operation is reduced by only 2% when compared to the protein free case; when the BSA loading is raised to 50 kg / m^3 the reduction is 8%. The elimination of convection clearly does not

have as significant an impact as in the first set of simulations. However, since diffusive transport is the dominant transport mechanism in the second set of simulations, this observation was expected.

Note as well that the average ECS glucose concentration is virtually identical in the three series (see Figure 4.2.9). After half an hour of operation, the maximum glucose concentration of 3 kg / m^3 is attained all along the ECS. Unlike in the first set of simulations, the presence of protein has a negligible affect on insulin production.

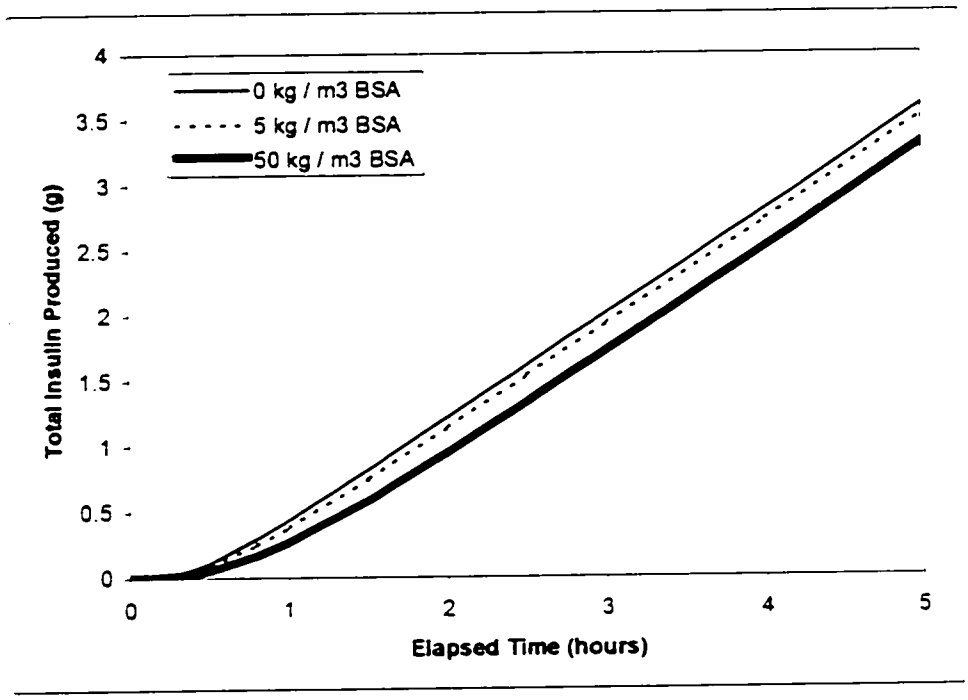

Figure 4.2.8 Total insulin produced by the high species permeability systems

The average insulin flux, meanwhile, is presented in Figure 4.2.10. This figure shows that the insulin responses of the three simulations are much closer than those observed in the first set of simulations. However, the insulin response is still quickest when no protein is present.

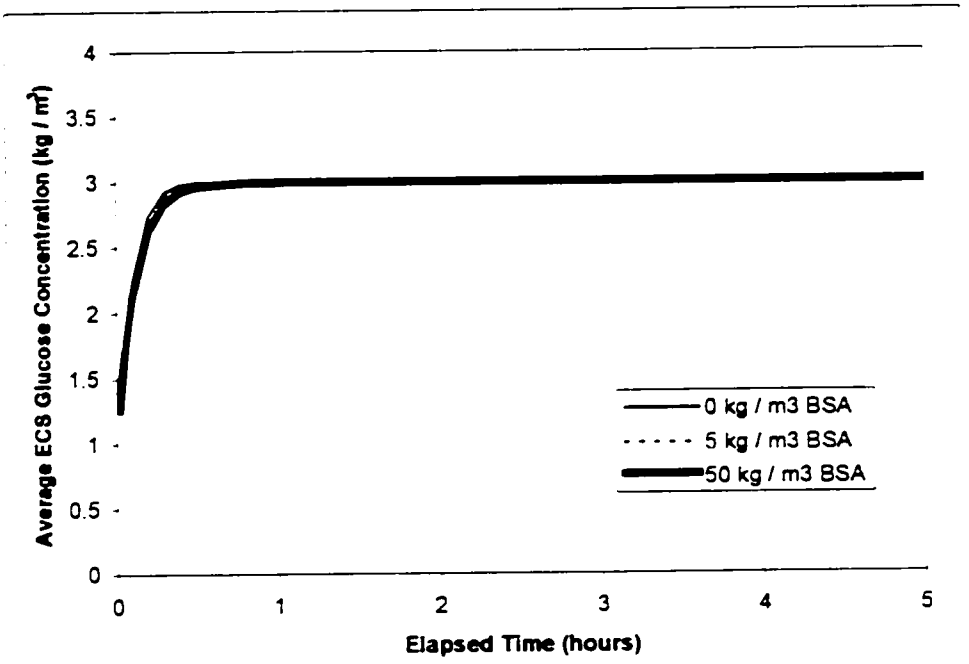

Figure 4.2.9 Average ECS glucose concentration for the high permeability systems

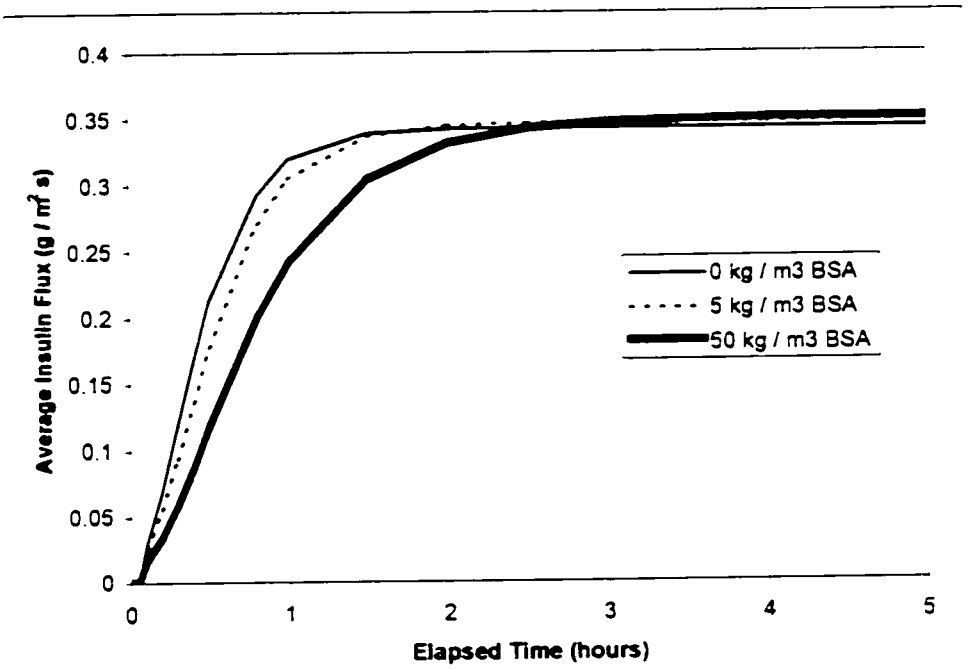

Figure 4.2.10 Average insulin flux for the high species permeability systems

When a high degree of convection is present, the insulin is quickly "washed out" of the ECS. However, when mass transfer occurs primarily by diffusion, the trans–membrane concentration gradient becomes the principal driving force behind mass transfer. Consequently, the insulin must accumulate in the ECS before a significant flux is observed. Eventually the concentration builds up to a point where the insulin flux attains steady-state and reaches that found in the first series.

Finally, it is noted that the insulin flux profiles after five hours of operation are similar to those observed in the first set of simulations (see Figure 4.2.11). By increasing the species permeabilities, the diffusive flux of insulin across the membrane is also increased. Since diffusive insulin mass transfer to the lumen occurs all along the device when 50 kg / m^3 of BSA is present in the ECS, the increase in permeability has a greatest impact under these operating conditions. For this reason, the performance of the device was not as significantly impaired by polarisation at the higher species permeabilities. However, the device response was still significantly quicker when convection was present

Since protein polarisation may cause a significant reduction in device performance for systems that rely on convective mass transfer, its elimination could certainly be advantageous. Protein polarisation could be eliminated by periodically alternating the flow direction. This solution was attempted by Piret and Cooney. It was found that lactate production for a reactor with a cycle time of 10 minutes was about twice that of a reactor operating with the flow in a single direction (Piret & Cooney 1990). Flow cycling could also prove beneficial to the high species permeability system. Polarisation of growth factors could reduce cell growth and in turn reduce the long term productivity of the device.

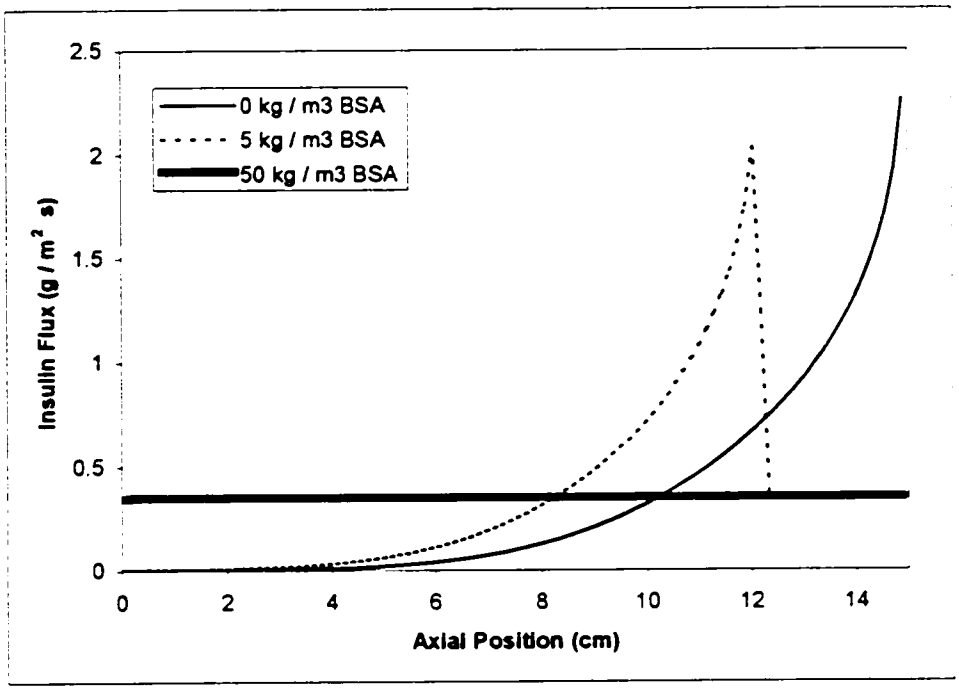

Figure 4.2.11 Insulin flux after 5 hours of operation for the high species permeability systems

4.3 Liver

The bioartificial pancreas' mathematical model was extended to the bioartificial liver by adjusting the kinetics to describe those of hepatocytes. The two species studied here, ammonia and n-caproic acid, are eliminated by the hepatocytes according to a pseudo first order consumption term (see Equation 2.4.12). The consumption is also a function of the viable cell density; however, this value is assumed to be independent of the local ammonia and n-caproic acid concentrations.

Instead of performing simulations at high and low species permeabilities, the effect of protein polarisation on start-up and steady-state operation of a bioartificial liver was investigated. Device performance was simulated under two operating regimes: a quasi steady-state condition in which the levels of ammonia and n-caproic acid throughout the device were initially equal to those in the lumen inlet, and a transient case in which the ECS was initially free of these two species. The first simulations were

undertaken under quasi steady-state conditions at three levels of BSA in the ECS. Under these conditions, there is no build-up of ammonia or n-caproic acid in the ECS. The second set of simulations considered the transient build-up of species concentration in the ECS.

The parameters common to all simulations are listed in Table 4.3.1. The osmotic relationship and virial coefficients were taken from Patkar *et al.* 1995 while membrane parameters were taken from Fujii & Kigoshi 1994. All other parameters were taken from Ohshima *et al.* 1994. There is a dearth of hepatocyte kinetic information. This last article was the only one that presented usable kinetic data.

Quasi Steady-State Conditions

In the case of the bioartificial liver, the device performance was gauged by calculating the difference between the species inlet and outlet flow rates. Unlike the bioartificial pancreas where glucose stimulates insulin production, in the bioartificial liver ammonia and n-caproic acid enter the device and stimulate their own consumption. Equation 4.3.1 calculates the consumption rate at time t while Equation 4.3.2 calculates the total species consumption after t seconds of operation.

$$\dot{m}_x(t) = \pi r_1^2 \left(\bar{u}_L(0,t) \bar{C}_{xL}(0) - \bar{u}_L(L,t) C_{xL}(L,t) \right) \tag{4.3.1}$$

$$\sum_{t=0}^{t} \dot{m}_x(t) \Delta t \tag{4.3.2}$$

Figures 4.3.1 and 4.3.2 both show that the presence of protein in the ECS significantly impaired steady-state device performance, as measured by the cumulative consumption of the two waste solutes monitored here. The inlet and outlet velocities as well as the inlet concentrations were all constant values. The presence of protein therefore resulted in a higher species outlet concentration in the second and third simulations, when compared to those in the first simulation. This difference implies at

least one of the following conditions: (i) ammonia and n-caproic acid were consumed at a greater rate when no protein was present; (ii) there was less species accumulation in the ECS in the second and third simulations when compared to the first.

Table 4.3.1: Parameters common to all liver simulations (Patkar *et al.* 1995, Ohshima *et al.* 1994)

Parameter	Value
Ammonia diffusivity in the ECS (m^2 / s)	3.0×10^{-9}
n-caproic acid diffusivity in the ECS (m^2 / s)	1.2×10^{-9}
Ammonia diffusivity in the lumen (m^2 / s)	0
n-caproic acid diffusivity in the lumen (m^2 / s)	0
BSA diffusivity (m^2 / s)	1×10^{-10}
Initial lumen ammonia concentration (mol / m^3)	0.6
Inlet ammonia concentration (mol / m^3)	0.6
Initial lumen n-caproic acid concentration (Eq / m^3)	3.0
Inlet n-caproic acid concentration (Eq / m^3)	3.0
Fibre length (m)	0.15
Inner fibre radius (μm)	100
Outer fibre radius (μm)	140
Krogh cylinder radius (μm)	1700
Hydraulic permeability (m)	6.0×10^{-13}
Ammonia permeability (m / s)	9.4×10^{-8}
n-caproic acid permeability (m / s)	3.7×10^{-8}
Fluid velocity (cm / s)	3
BSA molecular weight (g / mol)	69000
Viscosity (Pa s)	0.000694
First osmotic virial constant A_2 (m^3 / kg)	10.473×10^{-3}
Second osmotic virial constant A_3 (m^6 / kg^2)	17.374×10^{-6}
Temperature (°K)	310
Cell death constant (1 / s)	1.81×10^{-5}
Initial cell density (cell / m^3)	5×10^{10}
Initial cell viability	0.8
Ammonia rate constant (m^3 / cell s)	5.556×10^{-16}
n-caproic acid rate constant (m^3 / cell s)	8.333×10^{-16}
Time step (s)	0.1
Number of control volumes	200
Simulation duration (hours)	5

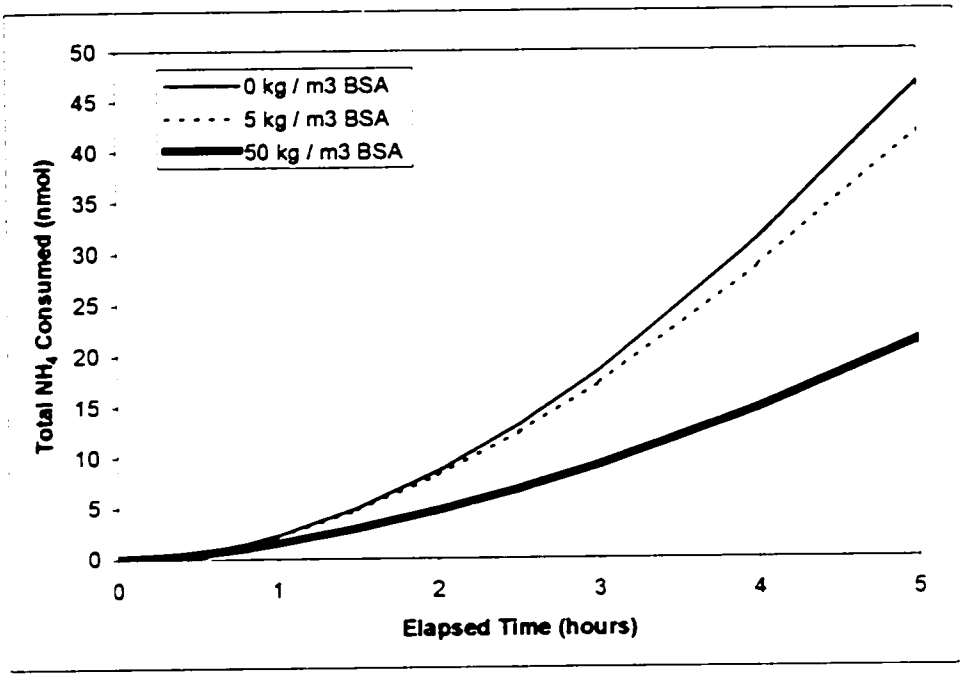

Figure 4.3.1 Total ammonia consumed during steady-state operation

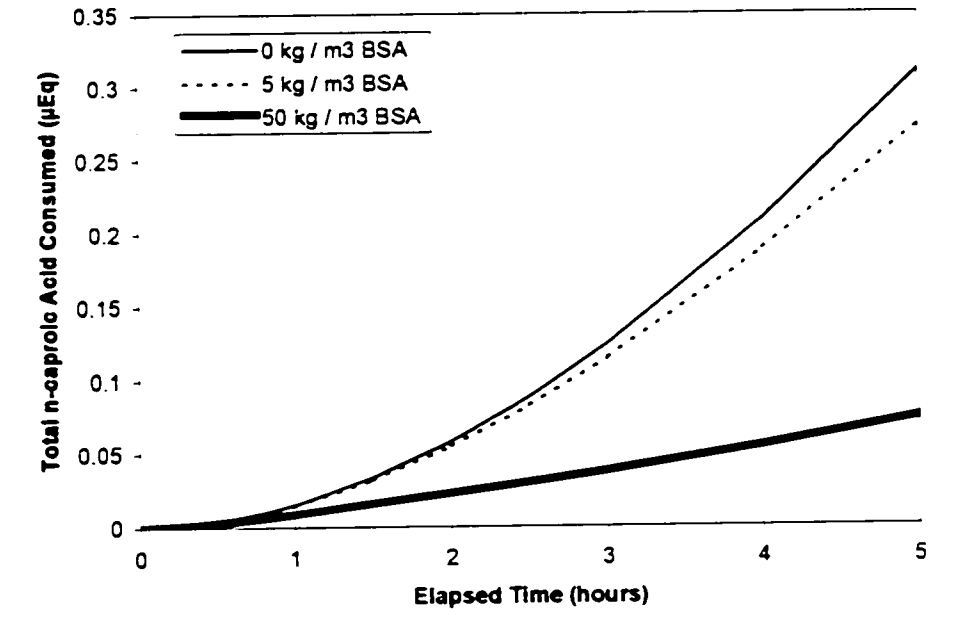

Figure 4.3.2 Total n-caproic acid consumed during steady-state operation

The average ECS ammonia and n-caproic acid concentrations were plotted as a function of the elapsed time. Figures 4.3.3 and 4.3.4 show that there was little difference between the average ECS concentrations in each of the three series. Since the concentrations are about the same, their rate of consumption will also be similar.

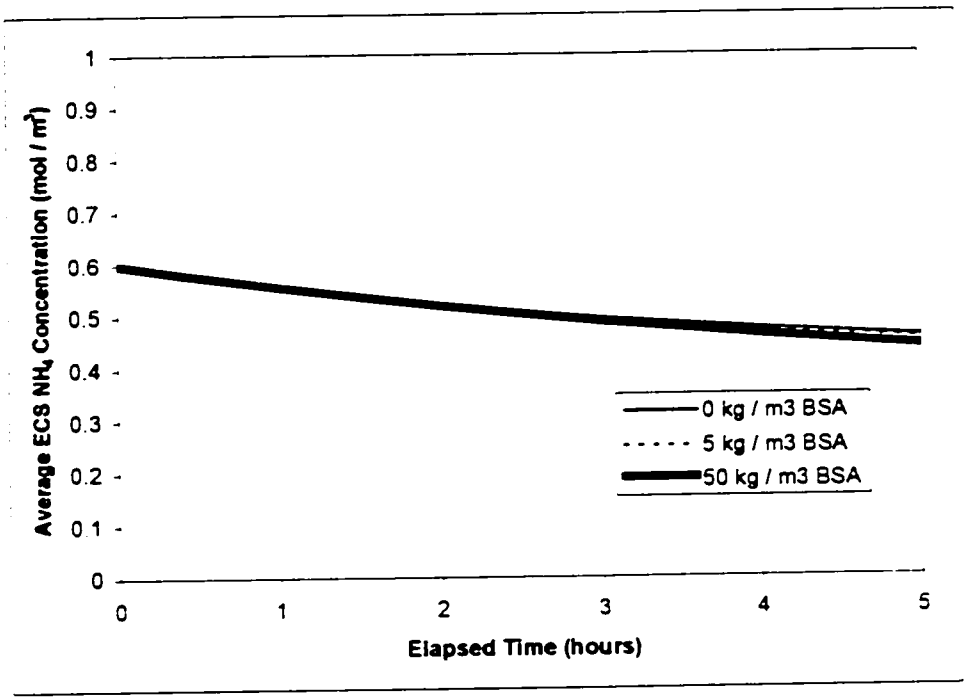

Figure 4.3.3 Average ECS ammonia concentration for the steady-state systems

The slight difference in average ammonia and n-caproic acid ECS concentration between the two simulations helps to explain the difference in output observed in Figures 4.3.1 and 4.3.2. In the three simulations, the same amount of ammonia and n-caproic acid entered the device. Since the two species concentrations in the ECS after five hours of operation were slightly higher when no protein was present, this small accumulation accounted for some of the apparent "consumption" observed. As shown in Equation 4.3.3, the total amount of ammonia and n-caproic acid in the ECS can be calculated by multiplying the ECS volume by the average species concentration.

$$N_{xE} = \overline{C}_{xE\,Average}\left(\pi r_3^2 - \pi r_2^2\right)L \qquad (4.3.3)$$

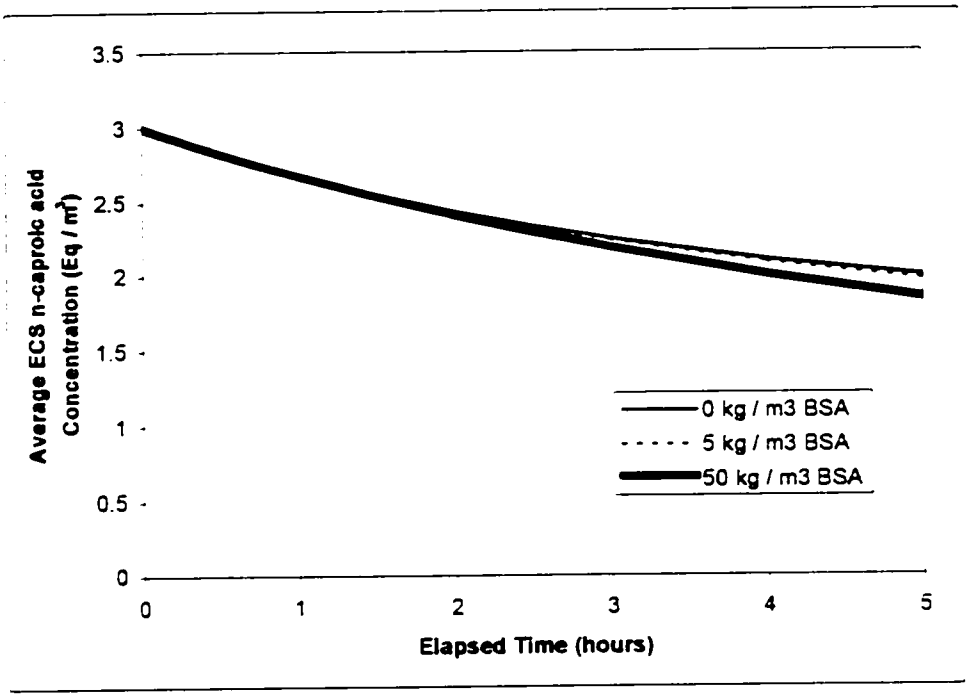

Figure 4.3.4 Average ECS n-caproic acid concentration for the steady state systems

The first simulation's total ECS ammonia content after five hours is 23.11 nmoles higher than the value obtained for the third simulation. Figure 4.3.1, meanwhile, indicates that the difference in consumption between these two simulations is 25.35 nmoles. For n-caproic acid these values are 0.21 and 0.24 μEq respectively. These results indicate that over 85% of the difference in device performance can be attributed to accumulation of solute species in the ECS. Although the slightly higher concentrations in the ECS in the first simulation do result in slightly higher consumption rates, this effect accounts for only a minimal part of the performance differences observed in Figures 4.3.1 and 4.3.2.

The reason for the slightly higher ECS species concentrations in the first simulation can be understood by looking at the fluid flux and BSA concentration profiles in Figures 4.3.5 and 4.3.6. In the high convection system (with no protein), the delivery of ammonia and n-caproic acid to the ECS is independent of the concentration gradient across the membrane. When convective flow to the membrane is shut down, transfer of

these two species occurs solely by diffusion. Diffusive transport is driven by the concentration gradient. Since the concentrations in the ECS and lumen are very close, (they are initially identical) the delivery of these species to the ECS will be slower than in the high convection system. This will lead to a lower ECS ammonia and n-caproic acid concentration.

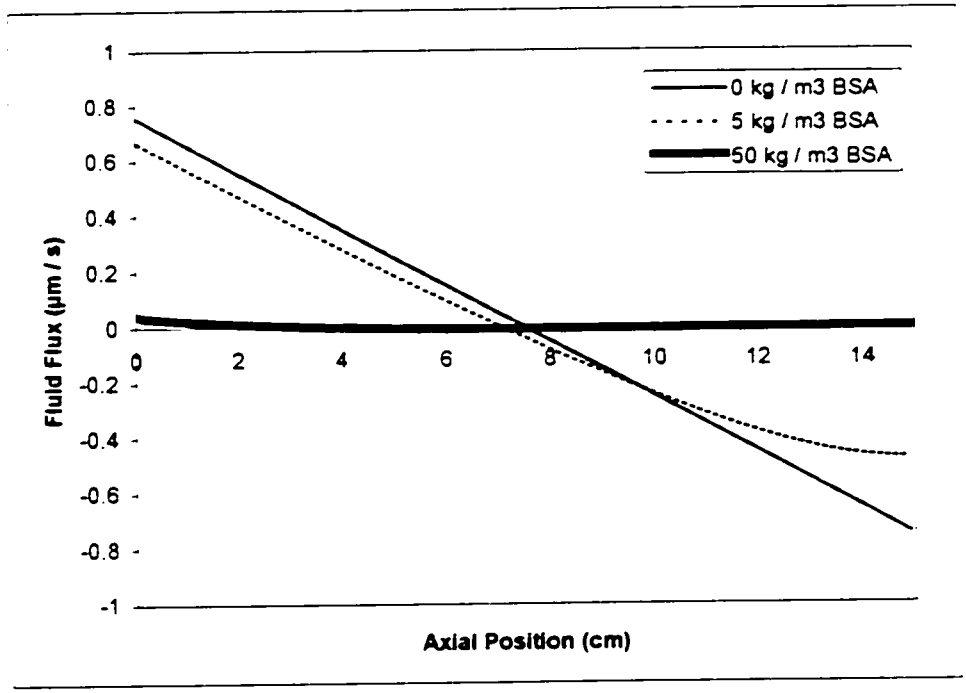

Figure 4.3.5 Fluid flux profiles after 5 hours of operation for the steady-state systems

Transient device operation

The second set of simulations was performed with different initial ECS species concentrations. The purpose of this change was to investigate device performance under start-up conditions. The initial ECS ammonia and n-caproic acid concentrations were 0. Therefore these two species must first enter the ECS before they can stimulate their own consumption. As the concentrations build up, the consumption rates also rise accordingly.

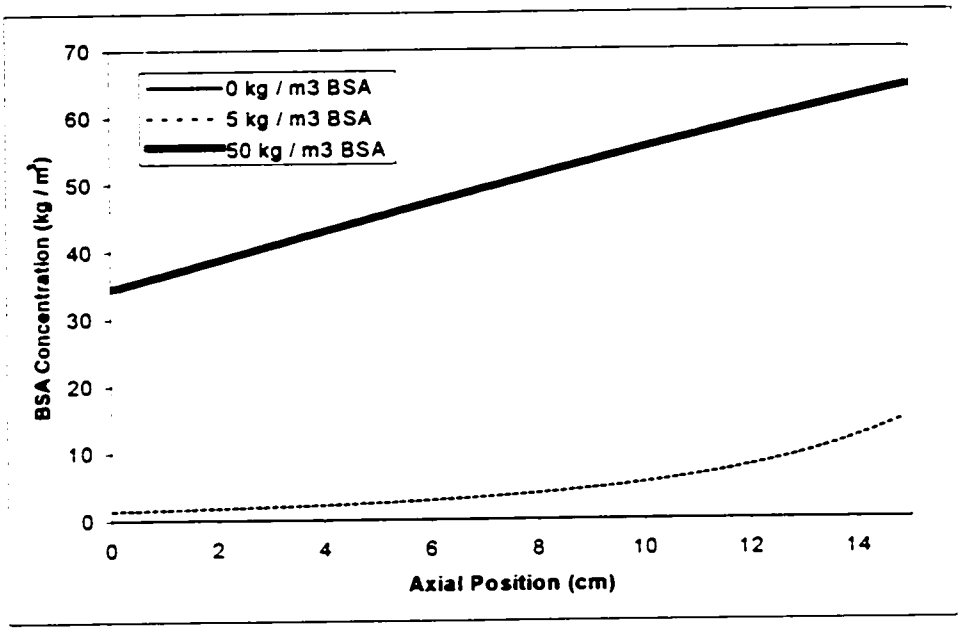

Figure 4.3.6 BSA Concentration profiles after 5 hours of operation for the steady-state systems

Figures 4.3.7 and 4.3.8 show the device performance curves for a system at the two extreme cases: one without any protein and for one loaded with 50 kg / m^3 of BSA. The curves are similar to those obtained in Figures 4.3.1 and 4.3.2. The uptake of ammonia and n-caproic acid after five hours of operation was about five times greater than the amount taken up under the quasi steady-state conditions. The reason can be attributed to greater ECS species accumulation in the former case.

Figures 4.3.9 and 4.3.10 show the average ECS ammonia and n-caproic acid concentrations as a function of elapsed time. Unlike the results in the previous set of simulations, the concentrations were much higher when no protein was present. Once again, the difference in ECS concentration helps to explain the performance differences between the two series. The difference in ammonia ECS accumulation after five hours of operation was 125 nmoles. The difference in total output was 142 nmoles. Since the ECS ammonia concentration was higher when no protein was present, an additional 17 nmoles of ammonia was consumed. For n-caproic acid, these values were 0.75 and 0.91 μEq. The difference that can be attributed to increased consumption is 0.16 μEq.

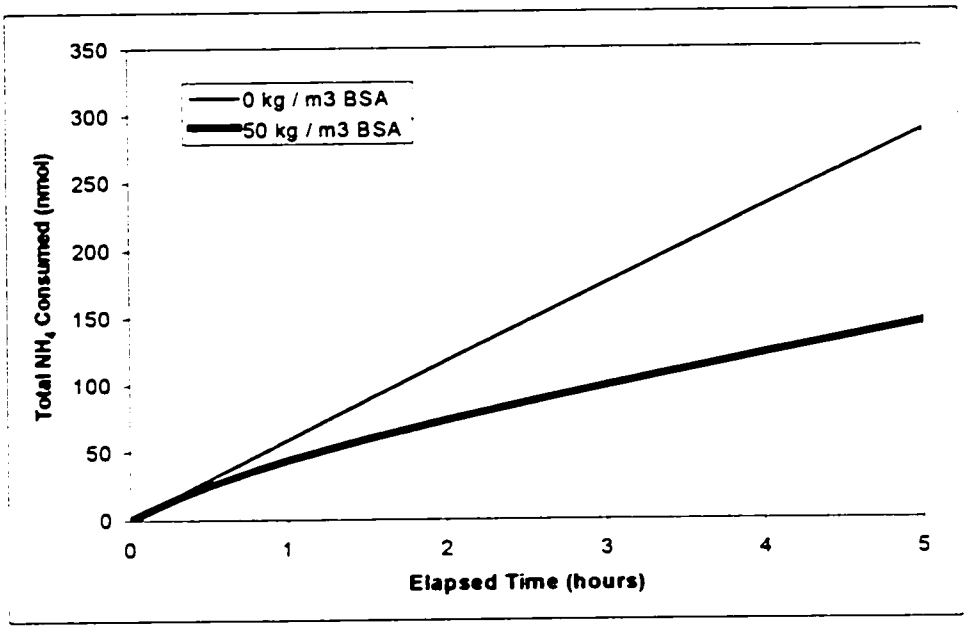

Figure 4.3.7 Total ammonia consumed during transient operation

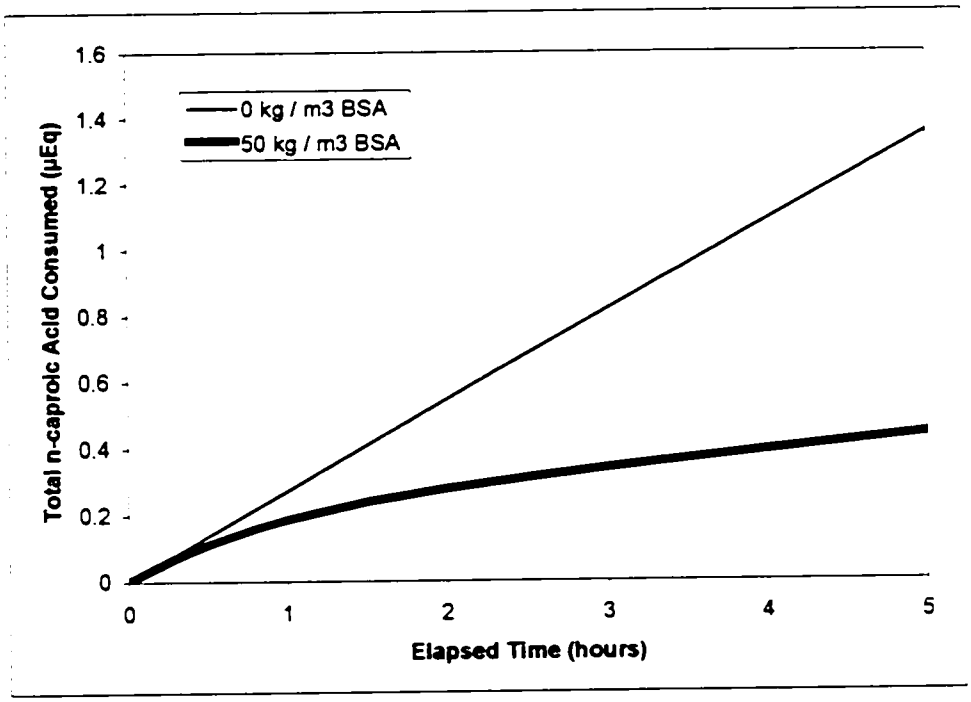

Figure 4.3.8 Total n-caproic acid consumed during transient operation

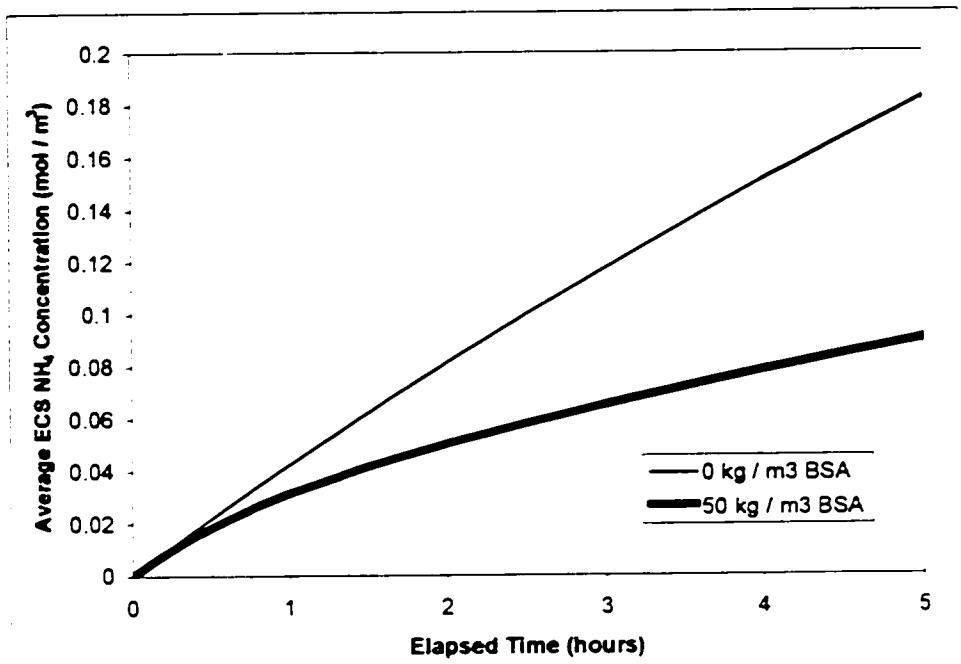

Figure 4.3.9 Average ECS ammonia concentration for the transient systems

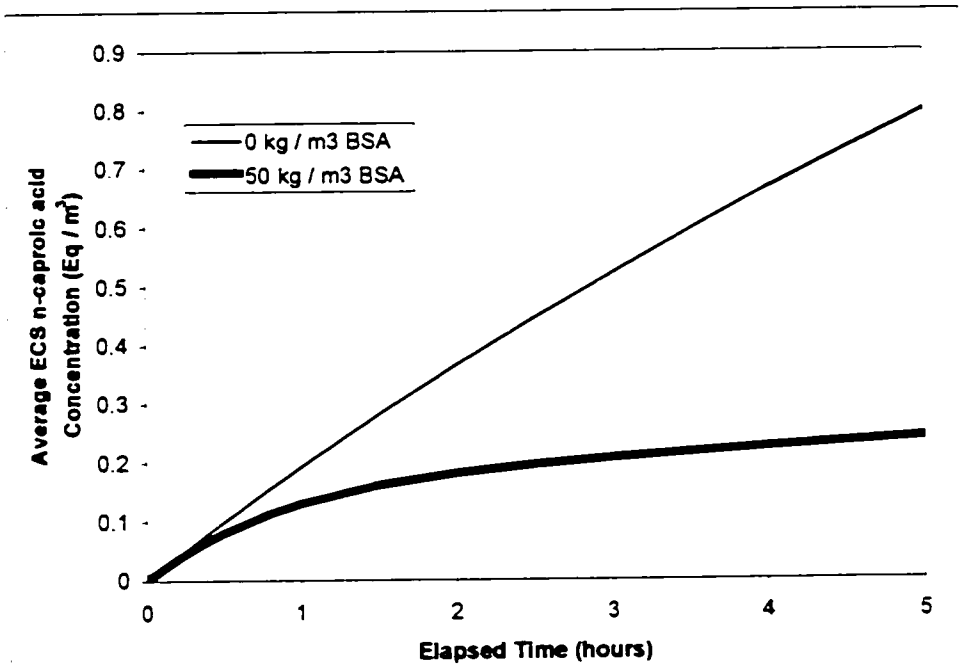

Figure 4.3.10 Average ECS n-caproic acid concentration for the transient systems

The difference in ammonia and n-caproic acid removal for the two systems can once again be attributed to the difference in their fluid flux and BSA concentration profiles. Since none of the hydrodynamic parameters have been changed, the profiles found in Figures 4.3.5 and 4.3.6 are applicable to these simulations. The difference in the species flux profiles is quite striking. Figures 4.3.11 and 4.3.12 show that when convective transport is present, a large amount of ammonia and n-caproic acid is transported into the ECS. Unlike the steady-state condition, the species transport in the first half of the device is not offset by the reverse flow in the downstream end. (There is little ammonia or n-caproic acid in the ECS at this point in time, so only a small amount is removed in the downstream end of the device.) The flux in the protein loaded device, meanwhile, occurs almost exclusively by diffusion and is fairly uniform across the length of the device.

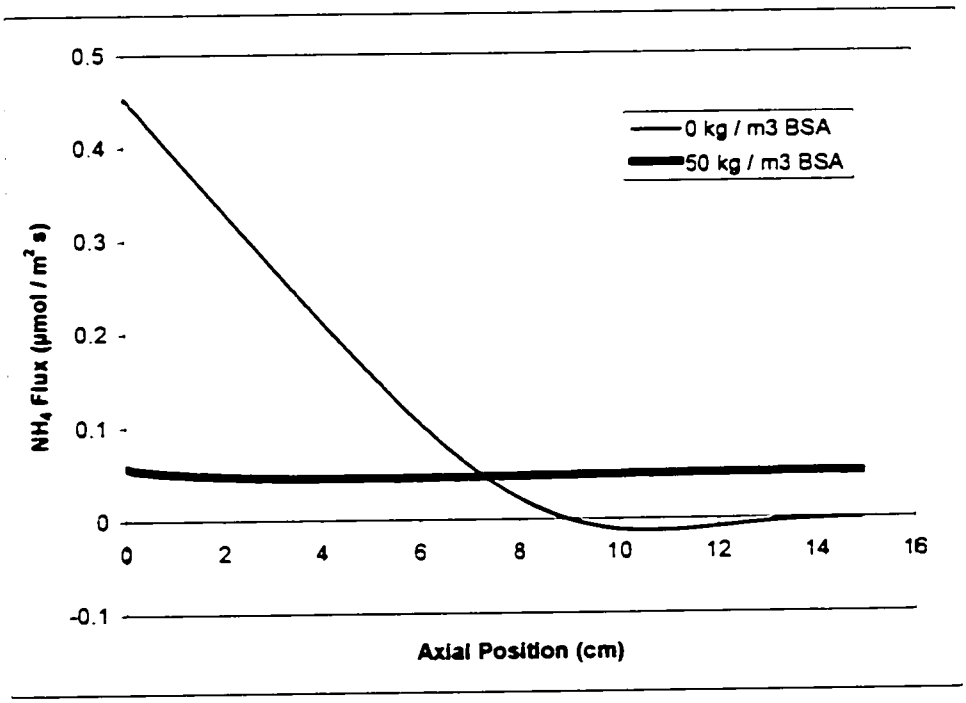

Figure 4.3.11 Ammonia flux profiles after five hours of operation for the transient systems

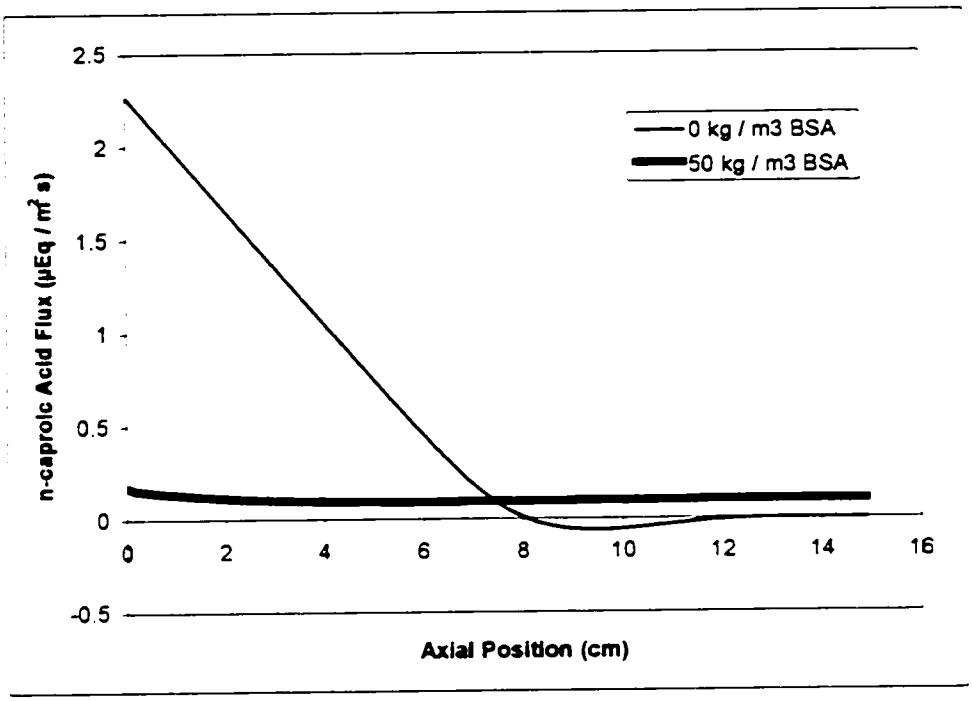

Figure 4.3.12 n-caproic acid flux profiles after five hours of operation for the transient systems

The performance difference caused by species build-up in the ECS may shed some light on some of the performance issues governing bioartificial liver operation. Most of the device performance obtained during device start-up is caused by species build-up in the ECS. As the ECS concentrations rise, the device performance eventually decreases. This is apparent when the performance curves in Figures 4.3.1, 4.3.2, 4.3.7 and 4.3.8 are compared. This performance decrease would be in addition to that caused by cell death. The build-up of ECS concentrations would also have a deleterious effect on the production of growth hormones and other factors required by the body.

The results shown here seem to indicate that it is not sufficient to measure device performance by simply measuring the difference in input and output toxin concentration. Species accumulation in the ECS could be mistaken for actual consumption. Once the ECS concentration values rise to those found in the blood stream, hepatocyte performance would appear reduced even though the difference is actually hydrodynamic.

Chapter 5

Conclusions and Recommendations

The results obtained in the simulations indicate that convective transport across the membrane can improve hollow fibre bioartificial organ device performance and the presence of an osmotically active excluded protein in the extra capillary space (ECS) can reduce or even effectively eliminate convective transport across the membrane.

The bioartificial pancreas simulations showed that for systems where convection is the dominant mass transfer mechanism, protein polarisation significantly impaired device performance by reducing the transport of glucose to the ECS and by reducing the rate of insulin delivery into the bloodstream.

When species diffusion across the membrane played a more significant mass transfer role, the effect of protein polarisation on insulin delivery to the bloodstream was significantly reduced. However, the device response was still quicker when no protein was present.

In the case of the bioartificial liver, protein polarisation resulted in an apparent reduction of ammonia and n-caproic acid consumption. Most of the performance increase observed for a system where trans-membrane convection is an important mass transfer mechanism (when no protein is present) is due to species accumulation in the ECS. The convective flux particularly improved device performance during start-up conditions where a build-up of ammonia and n-caproic acid was required.

It is important to note the weakness of the current state of liver kinetic models. The models used in this thesis were taken from Ohshima *et al.* 1994. Although they provide an adequate first step, many issues are ignored. Cell viability was simply a function of time. In all simulations, after five hours of operation, the cell viability dropped from 0.8 to 0.57. This model, however, does not incorporate the impact of nutrient depletion or toxin accumulation on cell viability. Ammonia is a toxic substance and, while one of the hepatocytes' functions is its elimination, a high level of ammonia

will reduce cell viability (Catapano & De Bartolo 1996). The current model does not account for this.

The multi-factorial nature of liver cell reactions also complicates the study of hepatocyte kinetics. As an example, it is known that oxygen concentration has a profound effect on hepatocyte viability and the rate at which they synthesise urea (Catapano & De Bartolo 1996). The simple approach of developing a kinetic model that assumes that the consumption rate of a toxin is linearly related to its concentration is crude at best. Significant experimental and theoretical research is therefore required to develop better models that can properly predict hepatocyte behaviour. A rectilinear flow cell that mimics hollow fibre bioreactor operation has been developed in our lab and could be used for this purpose (Pomalis & Taylor 1997).

Chapter 6

Glossary

Allogeneic Cells	Transplanted cells taken from an animal that is of the same species as the recipient
BAL	Bioartificial Liver
BAP	Bioartificial Pancreas
BSA	Bovine serum albumine. Protein common in cell culture medium. Albumine is also present in the blood
ECS	Extra capillary space. Space between the hollow fibres
Hepatocytes	Liver cells
HFBR	Hollow fibre bioreactor. Device composed of a bundle of hollow fibres that serve to isolate cell cultures from the blood stream
Islets of Langerhans	Pancreatic cells that secrete various hormones including insulin
LAD	Liver assist device
Lumen	Space inside the hollow fibres
N-caproic acid	A fatty acid eliminated by the hepatocytes
TDMA	Tri-diagonal-matrix-algorithm. Algorithm used to solve the control volume equations.
Xenogeneic Cells	Transplanted cells taken from an animal that is not of the same species as the recipient.

Chapter 7

References

Aębischer P., Wahlberg L., Tresco P., A. et al. "Macroencapsulation of dopamine secreting cells by coextrusion with an organic polymer solution", *Biomaterials* **12**, 50-56, (1991).

Agishi T., Kaneko I., Hasua Y., et al., "Double filtration for selective removal or retrieval of plasma fraction", *ASAIO Abstr.* **8**, 70, (1979).

Apelblat A., Katzir-Katchalsky A., Silberberg A., "A mathematical analysis of capillary-tissue fluid exchange", *Biorheology* **11**, 1-49, (1974).

Arnaout W. S., Moscioni A. D., Barbour R. L., et al., "Development of bioartificial liver: bilirubin conjugation in Gunn rats", *Journal of Surgical Research* **48**, 379-382, (1990).

Aung T., Kogire M., Inoue K., et al., "Insulin release from a bioartificial pancreas using a mesh reinforced polyvinyl alcohol hydrogel tube", *ASAIO Journal* **39**, 93-96, (1993).

Bejan A., "Heat transfer", *John Wiley & Sons*, 148-155, (1993).

Bodziony J., "Bioartificial endocrine pancreas: foreign-body reaction and effectiveness of diffusional transport of insulin and oxygen after long term implantation", *Research In Experimental Medicine* **192**, 305-316, (1992).

Bodziony J., Deeg M., Fricke O., et al., "Isolation of islets from the pig pancreas and their short-term use in an extracorporeal bioartificial pancreas in rats", *Transplantation Proceedings* **26**, 1095-1096, (1994).

Braun K., Besch W., Jahr H., et al., "The encapsulation of pancreatic islets, investigation of insulin secretion and content in-vitro", *Biomed. Biochim. Acta* **44**, 143-147, (1985).

Castano L., Eisenbarth G. S., "Type I diabetes: a chronic autoimmune disease of the human, mouse and rat", *Annu Rev. Immunol* **8**, 647-679, (1990).

Catapano G., "Mass transfer limitations to the performance of membrane bioartificial liver support devices", *International Journal of Artificial Organs* **19**, 18-35, (1996).

Catapano G., De Bartolo L., "Importance of the kinetic characterization of liver cell metabolic reactions to the design of hybrid liver support devices", *International Journal of Artificial Organs* **19**, 670-676, (1996).

Catapano G., Iorio G., Drioli E., et al., "Theoretical and experimental analysis of a hybrid bioartifical membrane pancreas: a distributed parameter model taking into account Starling fluxes", *Journal of Membrane Science* **52**, 351-378, (1990).

Cieslinski D. A., Humes D. H., "Tissue engineering of a bioartificial kidney", *Biotechnology and Bioengineering* **43**, 678-681, (1994).

Cole D. R., Waterfall M., McIntyre M., et al., "Transplantation of microcapsules (a potential bio-artificial organ): biocompatibility and host reaction", *Journal of Materials Science* **4**, 437-442, (1993).

Colton C. K., Avgoustiniatos E. S., "Bioengineering in development of the hybrid artificial pancreas", *Journal of Biomechanical Engineering* **113**, 152-170, (1991).

Doyle F. J., Dorski C., Harting J. E., et al., "Control and modelling of drug delivery devices for the treatment of diabetes", *Proceedings of the American Control Conference* **10**, 776-780, (1995).

Dupuy B., Gin H., Baquey C., et al., "Agarose beads in paraffin oil as interfaces to encapsulate living cells. Tests of function with islets of Langerhans", *Artificial Organs* **11**, 314, (1987).

Fan M. Y., Lum Z. P., Fu X. W., et al., "Reversal of diabetes in BB rats by transplantation of encapsulated pancreatic islets", *Diabetes* **39**, 519-521, (1990).

Fitzgibbons S. J., "Making artificial organs work", *Technology Review*, 33-40, (1994).

Fujii Y., Kigoshi S., "Characterization of hollow-fibre membranes", *Journal of Chemical Engineering of Japan* **27**, 321-328, (1994).

Gerlach J., Kloeppel K., Mueller C., et al., "Hepatocyte aggregate culture technique for bioreactors in hybrid liver support systems", *International Journal of Artificial Organs* **16**, 843-6, (1993).

Gerlach J., Kloppel K., Schauwecker H. H., et al., "Use of hepatocytes in adhesion, and suspension cultures for liver support bioreactors", *International Journal of Artificial Organs* **12**, 788-792, (1989).

Giorgio T. D., Moscioni A. D., Rozga J., et al., "Mass transfer in a hollow fibre device used as a bioartificial liver", *ASAIO Journal* **39**, 886-892, (1993).

Grodsky G. M., "A threshold distribution hypothesis for packet storage of insulin and its mathematical modelling", *Journal of Clinical Investigation* **51**, 2047-2059, (1972).

Hager J. C., Carman R., Stoller R., et al., "A prototype for a hybrid artificial liver", *Trans. Amer. Soc. Artif. Int. Organs* **24**, 250-253, (1978).

Heath C. A., Belfort G., Hammer B. E., et al., "Magnetic resonance imaging and modelling of flow in hollow-fibre bioreactors", *AIChE Journal* **36**, 547-558, (1990).

Ip T. K., Aebischer P., "Renal epithelial cell controlled solute transport across permeable membranes as the foundation for a bioartificial kidney", *Artificial Organs* **13**, 58-65, (1989).

Jaffrin M. Y., Reach G., Notelet D., "Analysis of ultrafiltration and mass transfer in a bioartificial pancreas", *Journal of Biomechanical Engineering* **110**, 1-10, (1988).

Jarret R. J., Keen H., "Hyperglycemia and diabetes mellitus", *Lancet* **2**, 1009-1012, (1976).

Jauregui H. O., Gann K. L., "Mammalian hepatocytes as a foundation for treatment in human liver failure", *Journal of Cellular Biochemistry* **45**, 359-365, (1991).

Jayaraman V. K., "Solution of hollow fibre bioreactor design equations: the case of power law fluids", *The Chemical Engineering Journal* **55**, 73-75, (1994).

Kadletz M., Magometschnigg H., Minar E., et al., "Implantation of in-vitro endothelialized polytetrafluoroethylene grafts in human beings", *J. Thorac. Cardiovasc. Surg.* **104**, 736-742, (1992).

Kelsey L. J., Pillarella M. R., Zydney A. L., "Theoretical analysis of convective flow profiles in a hollow-fibre membrane bioreactor", *Chemical Engineering Science* **45**, 3211-3220, (1990).

Kiley J. E., Welch H. F., Pender J. C., et al., "Removal of blood ammonia by hemodialysis", *Proc. Soc. Exp Biol. Med.* **91**, 489-490, (1956).

Kincaid D., Cheney W., "Numerical analysis", *Brooks Cole Publishing Company*, 315-320, 541-543, (1991).

Klein E., Holland F. F., Eberle K., "Comparison of experimental and calculated permeability and rejection coefficients for hemodialysis membranes", *Journal of Membrane Science* **5**, 173-188, (1979).

Knazek R. A., Gullino P. M., Kohler P. O., et al., "Cell culture on artificial capillaries: an approach to issue growth in vitro", *Science* **178**, 65-67, (1972).

Kreslow M., Lum Z. P., Tai I. T., et al., "Xenotransplantation of microencapsulated fetal rat islets", Transplantation **51**, 651-655, (1991).

Labecki M., Piret J. M., Bowen B. D., "Two dimensional analysis of fluid flow in hollow-Fibre modules", *Chemical Engineering Science* **50**, 3369-3384, (1995).

Langer R., Vacanti J. P., "Tissue engineering", *Science* **260**, 920-926, (1993).

Langsdorf L. J., Krankel L. G., Zydney A. L., "Effect of blood-membrane interactions on solute clearance during hemodialysis", *ASAIO Journal* **39**, 767-772, (1993).

Lemanski J., Lipscomb G. G., "Effect of shell-side flows on hollow-fibre membrane device performance", *AIChE Journal* **41**, 2322-2326, (1995).

Levesque L., Brubaker P. L., Sun A. M., "Maintenance of long term secretory function by microencapsulated islets of Langerhans", *Endocrinology* **130**, 644-650, (1992).

Lin T. Y., Lee C. S., Chen C. C., et al., "Regeneration of human liver after hepatic lobectomy studies by repeated liver scanning and repeated needle biopsy", *Ann. Surg.* **190**, 48-53, (1979).

Lum Z. P., Kreslow M., Tai I. T., et al., "Xenografts of rat islets into diabetic mice. An evaluation of new smaller capsules", *Transplantation* **53**, 1180-1183, (1992).

Lysaght M. J., "Evolution of hemodialysis membranes", *Dialysis Membranes: Structures And Predictions*, 1-10, (1995).

Malchesky P. S., "Nonbiological liver support: historic overview", *Artificial Organs* **18**, 342-347, (1994).

Malchesky P. S., Asanama Y., Zawicki I., et al., "On line separation of macromolecules by membrane filtration with cryogelation", *Artificial Organs* **40**, 205, (1980).

Malchesky P. S., Ouchi K., Piatkiewicz W., et al., "Membrane plasma filtration systems with multiple reactors for hepatic support", *Artificial Organs* **2**, 265-268, (1978).

Matsura K. N., Robles G. G., Huston H., et al., "Hybrid bioartificial liver in hepatic failure: preliminary clinical report", *Surgery* **101**, 99-103, (1987).

Mikos A. G., Papadaki M. G., Kouvroukoglou S., et al., "Mini review: islet tansplantation to create a bioartificial pancreas", *Biotechnology and Bioengineering* **43**, 673-677, (1994).

Moussy Y., Moussy F., "Analysis of glucose and insulin mass transfer in a novel 2-channel bioartificial pancreas", *Artif. Cells, Blood Subst. & Immob. Biotech.* **23**, 163-173, (1995).

Neuzil D. F., Rozga J., Moscioni A., et al., "Use of a novel bioartificial liver in a patient with acute liver insufficiency", *Surgery* **113**, 340-343, (1993).

Nosé Y., Usami M., Malchesky P. S., et al., "Clinical thermofiltration: initial application", *Artificial Organs* **9**, 425-429, (1985).

Nyberg S. L., Platt J. L., Shirabe K., et al., "Immunoprotection of xenocytes in a hollow fibre bioartitifical liver", *ASAIO Journal* **38**, 463-467, (1992).

Nyberg S. L., Shatford R. A., Madhusudan P. V., et al., "Evaluation of a hepatocyte entrapment hollow Fibre bioreactor: a potential bioartificial liver", *Biotechnology and Bioengineering* **41**, 194-203, (1993a).

Nyberg S. L., Shirabe K., Peshwa M. V., et al., "Extracorporeal application of a gel-entrapment, bioartificial liver: demonstration of drug metabolism and other biochemical functions", *Cell Transplantation* **2**, 441-452, (1993b).

Ohshima N., Shiota M., Kusano H., et al., "Kinetic analyses of the performance of a hybrid-type artificial liver support system utilizing isolated hepatocytes", *Materials, Science and Engineering CI* **93**, 79-85, (1994).

Ohzato H., Carretta M., Maki T., "Use of xenogeneic islets in hybrid artificial pancreas for treatment of diabetes without immunosuppression", *Transplantation Proceedings* **24**, 661-662, (1992).

Opolon P., Rapin J. R., Huguet C., et al., "Hepatic failure coma treated by polyacrylonitrile membrane hemodialysis", *Trans Am. Soc. Artif. Inter. Organs* **22**, 701-710, (1976).

Patankar S. V., "Numerical heat transfer and fluid flow", *Taylor & Francis*, (1980).

Pathak C. P., Sawhney A. S., Hubell J. A., "Rapid photopolymerisation of immunoprotective gels in contact with cells and tissue", *J. Am. Chem. Soc.* **114**, 8311-8312, (1992).

Patkar A. Y., Koska J., Taylor D. G., et al., "Protein transport in ultrafiltration hollow-Fibre bioreactors", *AIChE Journal* **41**, 415-425, (1995).

Pillarella M. R., Zydney A. L., "Theoretical analysis of the effect of convective flow on solute transport and insulin release in a hollow fibre bioartificial pancreas", *Journal of Biomechanical Engineering* **112**, 220-228, (1990a).

Pillarella M. R., Zydney A. L., "Effect of beta cell distribution on the performance of a bioartificial pancreas", *Trans. Amer. Soc. Artif. Int. Organs* **36**, 715-719, (1990b).

Piret J. M., Cooney C. L., "Mammalian cell and protein distributions in ultrafiltration hollow fibre bioreactors", *Biotechnology and Bioengineering* **36**, 902-910, (1990).

Pomalis R., Taylor G., "A fundamental study of Starling flow and protein redistribution within a cell-free rectilinear membrane flow device", Thesis submitted to the Department of Chemical Engineering of the University of Ottawa, (1997).

Press W. H., Teukolsky S. A., Vetterling W. T., Flannery B. P., "Numerical recipes", *Cambridge University Press*, 2nd ed., 745-751, (1992).

Ramirez C. A., López M., Stephens C. L., "In-vitro perfusion of hybrid artificial pancreas devices at low flow rates", *ASAIO Journal* **38**, 443-449, (1992).

Reach G., "Pancréas artificiels et bioartificiels pour le traitement du diabète sucré", *Diabète & Métabolisme* **20**, 183-193, (1994).

Reach G., "Pancreas bioartificiels: une solution a la xenogreffe d'ilots de Langerhans", *Pathologie Biologie* **41**, 225-229, (1993).

Reach G., "Vers un traitement du diabète autorégulé en boucle fermée", *Annales D'Endocrinologie* **56**, 43-48, (1995).

Ronco C., "Dialysis delivery versus dialysis prescription", *International Journal of Artificial Organs* **16**, 628-635 (1993).

Rozga J., Demitriou A. A., "Artificial liver: evolution and future perspectives", *ASAIO Journal* **41**, 831-837 (1995).

Rozga J., Williams F., Ro M. S., et al., "Development of a bioartificial liver: properties and function of a hollow fibre module inoculated with liver cells", *Hepatology* **17**, 258-265, (1993a).

Rozga J., Holzman M. D., Ro M. S., et al., "Development of a hybrid bioartificial liver", *Annals of Surgery* **217**, 502-511, (1993b).

Rozga J., Morsiani E., LePage E., et al., "Isolated hepatocytes in a bioartificial liver: a single group view and experience", *Biotechnology and Bioengineering* **43**, 645-653, (1994).

Salmon P. M., Libicki S. B., Robertson C. R., "A theoretical investigation of convective transport in the hollow-fibre reactor", *Chemical Engineering Communications* **66**, 221-248, (1988).

Scharp D. W., Lacy P. E., Santiago J. V., et al., "Results of our first nine intraportal islet allografts in type 1, insulin-dependent diabetic patients", *Transplantation* **51**, 76-85, (1991).

Schecter D. C., Nealon T. F., Gibbon J. H., "A simple extracorporeal device for reducing elevated blood ammonia levels", *Surgery* **44**, 892-897, (1958).

Schnider P. A., Hanson S. R., Price T. M., et al., "Durability of Confluent endothelial cell monolayers of small caliber vascular prostheses in vitro", *Surgery* **103**, 456-462, (1988).

Shatford R. A., Nyberg S. L., Meier S. J., et al., "Hepatocyte function in a hollow fibre bioreactor: a potential bioartificial liver", Journal of Surgical Research **53**, 549-557, (1992).

Shepard A. D., Eldrup-Jorgensen J., Keough E. M., et al., "Endothelial cell seeding of small caliber synthetic grafts in the baboon", *Surgery* **99**, 318-325, (1986).

Shibusawa K., Tago J., "Artificial kidney", *Saishin-igaku* **11**, 298-310, (1956).

Sparks R. E., Mason N. S., Finley T. C., et al., "Development, testing and modelling of an islet transplantation chamber", *Trans. Amer. Soc. Artif. Int. Organs* **28**, 229-231, (1982).

Sparks R. E., Mason N. S., Sharp D. W., "Biomaterials in bioartificial organs", *MacMillan Ed.*, 193-199, (1984).

Stevenson W. T. K., Sefton M. V., "Fundamentals of animal cell encapsulation and immobilization", *CRC Press*, 143-181, (1993).

Sussman N. L., Chong M. G., Koussayer T., et al., "Reversal of fulminant hepatic failure using an extracorporeal liver assist device", *Hepatology* **16**, 60-63, (1992).

Sussman N. L., Gislason G. T., Conlin C. et al., "The hepatix extracorporeal liver assist device: initial clinical experience", *Artificial Organs* **18**, 390-396, (1994).

Sussman N. L., Kelly J. H., "Improved liver function following treatment with an extracorporeal liver assist device", *Artificial Organs* **17**, 27-30, (1993).

Takeshita K., Ishibashi H., Suzuki M., et al., "High cell-density culture system of hepatocytes entrapped in a three-dimensional hollow fibre module with collagen gel", *Artificial Organs* **19**, 191-193, (1995).

Tansley G. D., "Aspects of non-Newtonian blood flow in prosthetic valve studies", *Automedica* **15**, 207-226, (1993).

Taylor D. G., Boukouris D., "Influencing hollow fibre bioreactor hydrodynamics through osmotic pressures - a model study", *Chemical Engineering Science* **50**, 1513-1517, (1995).

Taylor D. G., Piret J. M., Bowen B. D., "Protein polarisation in isotropic membrane hollow fibre bioreactors", *AIChE Journal* **40**, 321-323, (1994).

Todisco S., Calabro V., Iorio G., "A lumped parameter mathematical model of a hollow fibre membrane device for the controlled insulin release", *Journal of Membrane Science* **106**, 221-232, (1995).

Uchino J., Matsushita M., "Artificial liver: strategies for the rescue of patients with liver failure", *ASAIO Journal* **40**, 74-77, (1994).

Vanholder R., "Bioartificial pancreas and liver: a review", *International Journal of Artificial Organs* **14**, 398-402, (1991).

Warnock G. L., Rajotte R. J., "Critical mass of purified islets that induce normoglycemia after implantation into dogs", *Diabetes* **37**, 467, (1988).

Wolf C. F., Munkelt B. E., "Bilirubin conjugation by an artificial liver composed of cultured cells and synthetic capillaries", *Trans. Amer. Soc. Artif. Int. Organs* **21**, 16-27, (1975).

Wu F. J., Friend J. R., Lazar A., et al., "Hollow fibre bioartificial liver utilizing collagen-entrapped porcine hepatocyte spheroids", *Biotechnology and Bioengineering* **52**, 34-44, (1996).

Yeh H. M., Cheng T. W., "Concentration polarisation model for hollow-fibre membrane ultrafiltration", *Separation Science and Technology* **29**, 497-512, (1994).

Zydney A. L., "Bulk mass transport limitations during high flux hemodialysis", *Artificial Organs* **17**, 919-924, (1993).

Appendix 1

Program Validation

A1.1 Validation Procedure

Since no analytical solution is available for the complete problem of simultaneous convection, diffusion, mass transfer and reaction within the hollow fibre bioreactor, it is not possible to directly test the full program's results. Instead, the system must be simplified to yield results that can be solved analytically; this solution is then compared to that provided by the simulator under identical conditions. Through a judicious choice of simplifying assumptions the various aspects of the simulator can be independently tested. In this case seven different tests were designed to validate the numerical simulator.

A1.2 Steady State Convection Diffusion

The steady state convection diffusion equation is one of the simplest forms of the one-dimensional conservation equation (Patankar 1980). In this situation, the fluid velocity and species diffusivity are constants. Assuming fixed solute concentrations at either end of the domain, the resulting differential equation shown below can be integrated to yield Equation A1.2.2.

$$D_x \frac{d^2\overline{C}_x}{dz^2} = \overline{u}\frac{d\overline{C}_x}{dz} \qquad \text{(A1.2.1)}$$

$$\frac{\overline{C}_x - \overline{C}_{x0}}{\overline{C}_{xL} - \overline{C}_{x0}} = \frac{\exp(Peclet_x z/L) - 1}{\exp(Peclet_x) - 1} \qquad \text{(A1.2.2)}$$

In the above equation, C_{x0} is the concentration at point 0, C_{xL} is the concentration at point L. The Peclet number, meanwhile, is defined with equation A1.2.3.

$$Peclet_x = \frac{\overline{u}L}{D_x} \qquad \text{(A1.2.3)}$$

Figure (A1.2.1) compares the numerical solution to the analytical one given by equation (A1.2.2). Both series are indistinguishable and the maximum relative error was 5.4×10^{-5} %, indicating that the numerical simulator properly solved this simplified problem.

Table A1.2.1: Values used in the solution of equation A1.2.2

Variable	Value
$Peclet_x$	8
C_{x0} (kg / m^3)	30
C_{xL} (kg / m^3)	100
L (m)	1

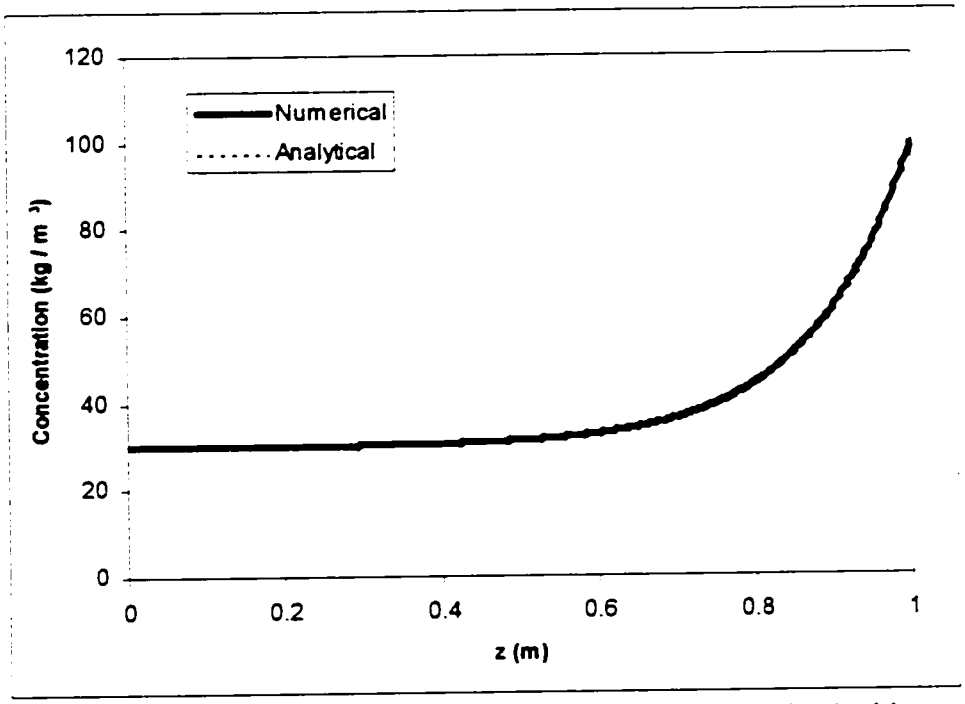

Figure A1.2.1 Steady-state convection-diffusion problem solved with the control volume method.

A1.3 Unsteady Conduction in a Rod

The previous test demonstrated that the program can properly calculate the impact of convection and diffusion. By solving the problem of unsteady heat conduction in a rod, it is possible to verify that the program can handle transient problems as well as steady-state problems. This latter problem is mathematically defined by the following differential equation (Bejan 1993):

$$\frac{\partial T}{\partial t} = \frac{1}{\varpi}\frac{\partial^2 T}{\partial z^2} \qquad \text{(A1.3.1)}$$

where ϖ represents the thermal diffusivity of the material, assumed here to be constant.

At time 0, the temperature at one end of the rod is raised. The problem can be solved by assuming that the temperature deep within the rod is unaffected by the increase in temperature at the surface of the rod, yielding the following analytical equation

$$\frac{T - T_\infty}{T_0 - T_\infty} = \mathrm{erf}\left[\frac{z}{2(\varpi t)^{1/2}}\right] \qquad \text{(A1.3.2)}$$

In this case T_∞ represents the rod's initial temperature while T_0 represents the elevated temperature at the rod's end.

Table A1.3.1: Values used in the solution of equation A1.3.2

Variable	Value
T_∞ (°C)	100
T_0 (°C)	30
ϖ (m^2 / s)	0.006

Again, the numerical solution was compared to the analytical solution (see Figure A1.3.1), testifying to the accuracy of the numerical solution. Note that, since the temperature deep within the rod has not changed, the semi-infinite boundary condition has not been violated.

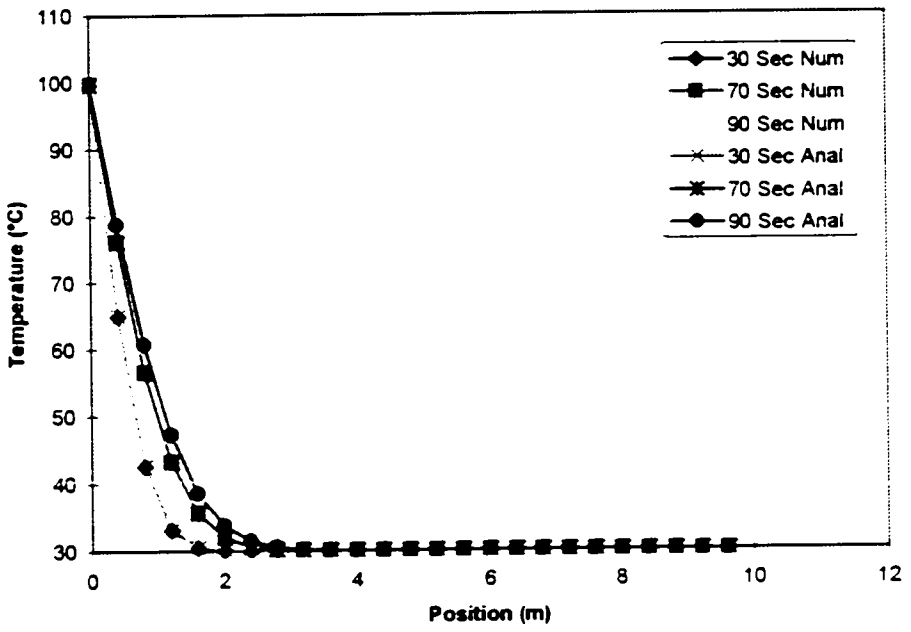

Figure A1.3.1 Unsteady heat conduction in a rod solved with the control volume method

A1.4 Velocity Calculation

The ECS fluid velocity is calculated with equation 2.3.8, which reduces to a linear 2nd order differential equation when protein polarisation is neglected. Integrating the linear equation yields the following analytical equation (Taylor *et al.* 1994):

$$\bar{u}_E(z) = \frac{r_1^2 \bar{u}_{L0}}{r_3^2 - r_2^2}\left(1 - \frac{\beta}{\lambda^2}\right)\left[1 - \frac{\cosh[\lambda(L/2 - z)]}{\cosh(\lambda L/2)}\right] \qquad \text{(A1.4.1)}$$

where

$$\lambda = \left[\frac{16L_P}{r_1^3}\left(1+\alpha r_1^4\right)\right]^{1/2} \qquad \text{(A1.4.2)}$$

$$\beta = 16\alpha r_1 L_P \qquad \text{(A1.4.3)}$$

$$\alpha = \left[4r_3^4 \ln(r_3/r_2) - \left(r_3^2 - r_2^2\right)\left(3r_3^2 - r_2^2\right)\right]^{-1} \qquad \text{(A1.4.4)}$$

The numerical results from this simplified problem were plotted alongside those obtained from equation A1.4.1. Table A1.4.1 lists the values used for the parameters of the above equation. Again, the figure shows that the numerical procedure properly calculated the ECS velocity.

Table A1.4.1: Values used in the solution of equation A1.4.1

Variable	Value
L (m)	0.15
L_P (m)	2.9×10^{-12}
r_1 (m)	0.0005
r_2 (m)	0.00067
r_3 (m)	0.0014
u_{l0} (m / s)	0.7491

A1.5 Flux Calculation

To ensure that the system satisfies continuity, the fluid that enters the ECS should be offset by the fluid exiting it. No net accumulation (or loss) of fluid should be observed. This can be determined by summing the fluid flux values in all of the control volumes. The ratio of this summation over the value of the flux at the first control volume should be virtually 0. The first control volume was chosen as a constant reference point. (The flux at the midpoint could not be used as a reference value because

its value tends towards 0; furthermore the midpoint shifts when polarisation occurs). This process yielded a summation value of -5.28×10^{-17} m / s. The flux at the first control volume was 3.87×10^{-6} m / s. From these values, we obtain a relative error of 2.75×10^{-9} %, confirming continuity of fluid is satisfied by the simulator.

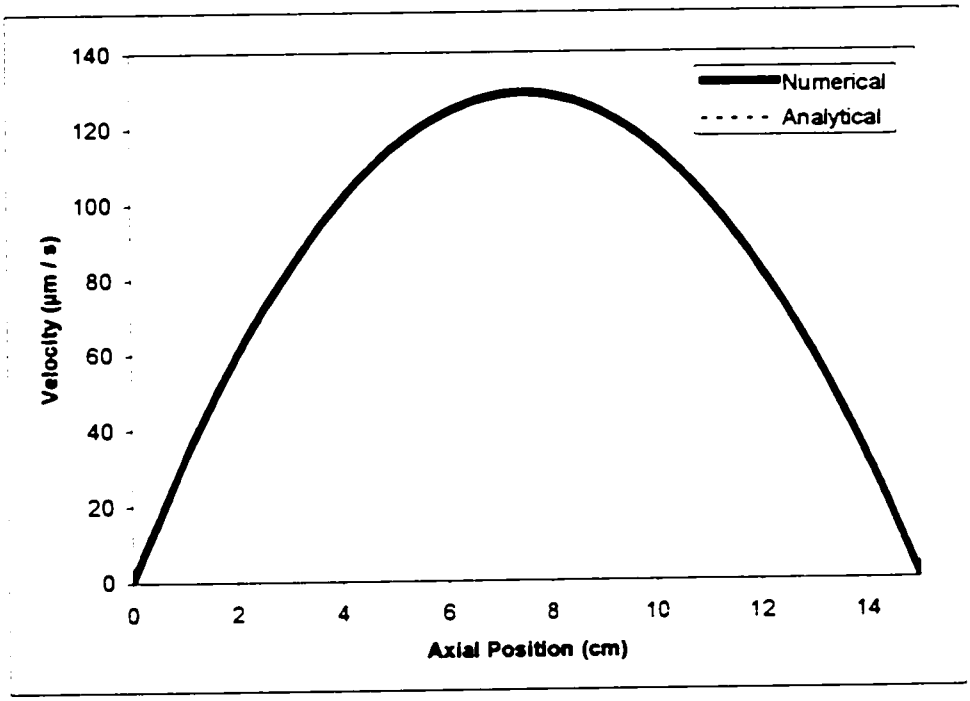

Figure A1.4.1 ECS fluid velocity without protein polarisation

A1.6 Pancreas Reaction Term

The reaction term can be tested by setting all velocities, diffusivites and permeabilities to 0. (Under these conditions there are no mass transfer effects.) An initial glucose concentration was chosen and the insulin generation calculated. The following table compares the analytical and numerical solutions and demonstrates that the program properly calculated the insulin generation.

Table A1.6.1: Results of the pancreas reaction term test

Time (seconds)	*Insulin – numerical (kg m^3)*	*Insulin – analytical (kg m^3)*	*Error (%)*
10	5.6451613	5.6451613	3.5×10^{-13}
20	10.602152	10.602152	4.32×10^{-12}

A1.7 Liver Reaction Term

A similar procedure to that listed in section A1.6 can be applied to the liver reaction term. In this case, two reaction terms are present. Table A1.7.1 summarises the results for the ammonia calculations while Table A1.7.2 summarises those for the n-caproic acid calculations. The results show that both reaction terms were properly calculated.

Table A1.7.1: Results of the ammonia reaction term test

Time (seconds)	*NH_4 – numerical (mol m^3)*	*NH_4 – analytical (mol m^3)*	*Error (%)*
10	0.557854649	0.557854649	2.99×10^{-13}
20	0.518675766	0.518675766	7.06×10^{-13}

Table A1.7.2: Results of the n-caproic acid reaction term test

Time (seconds)	*n-caproic acid numerical (Eq m^3)*	*n-caproic acid analytical (Eq m^3)*	*Error (%)*
10	2.694667554	2.694667554	9.39×10^{-13}
20	2.420452212	2.420452212	1.83×10^{-14}

A1.8 Grid Sensitivity

An important consideration when approximating a solution with a numerical method is its grid sensitivity. In a transient one-dimensional problem, the solution may depend on the size of the time step or on the width of the control volumes. The impact of these two terms is measured by comparing the results obtained with a coarse grid to those obtained with a finer grid. If no significant change is observed, the grid is sufficiently accurate. The overlapping curves in the following figures indicate that the coarser grids yield sufficiently accurate solutions for this system. These values were obtained from the high convection systems. The rate of change is greatest when there is a large amount of convection. This ensures that the grid is acceptable for all simulations.

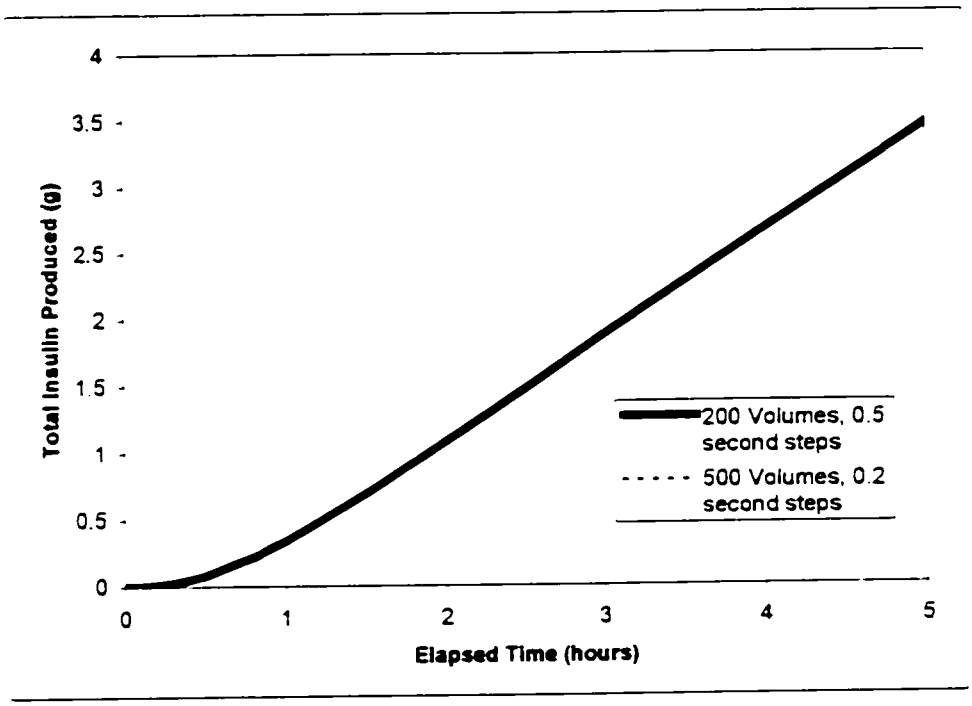

Figure A1.8.1 Pancreas grid sensitivity result

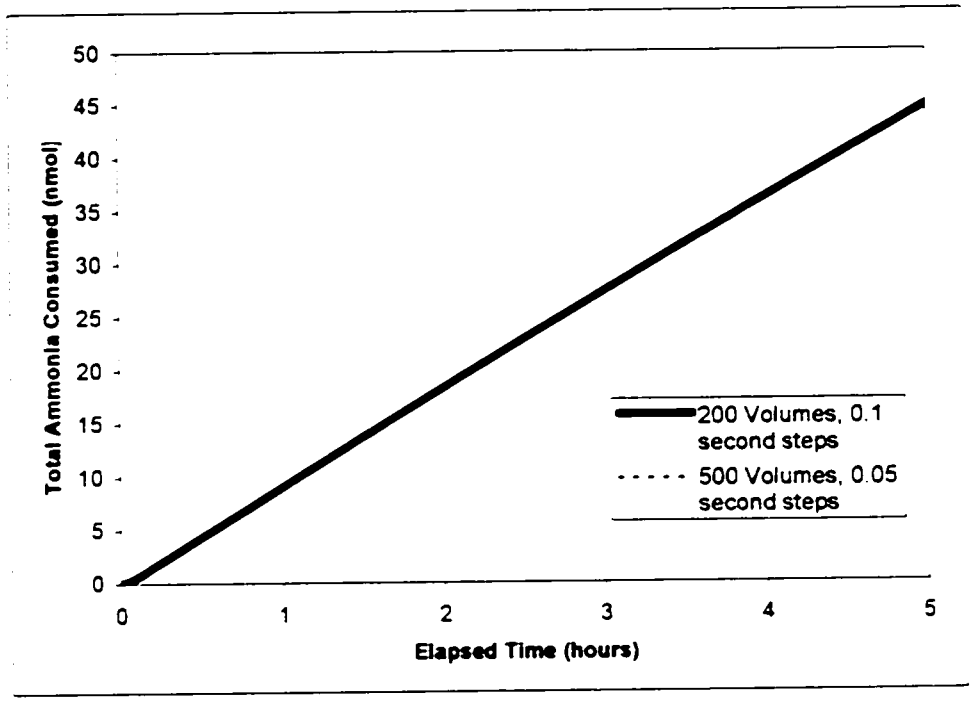

Figure A1.8.2 Liver grid sensitivity result (ammonia consumption)

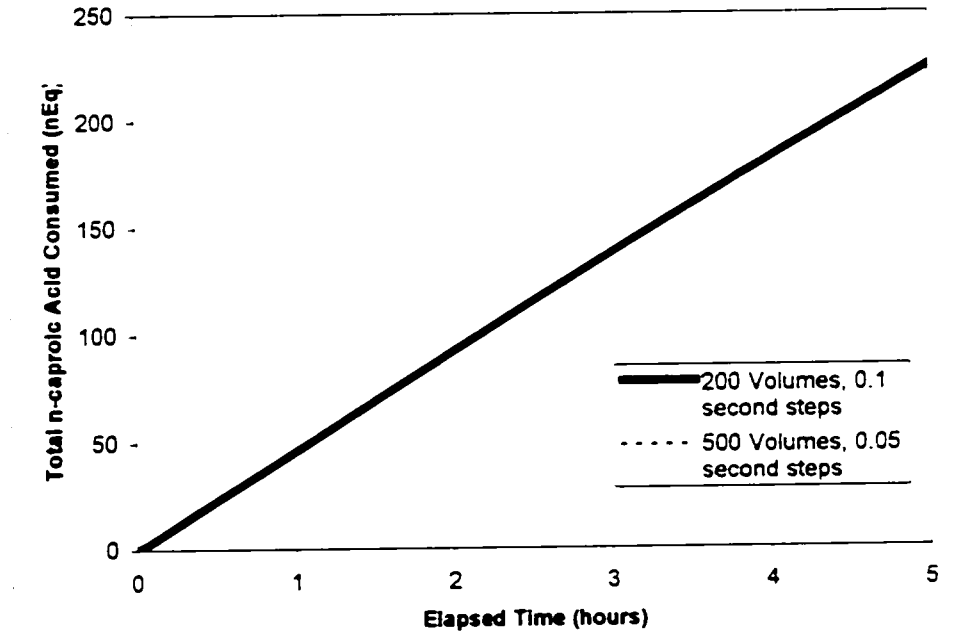

Figure A1.8.3 Liver grid sensitivity result (n-caproic acid consumption)

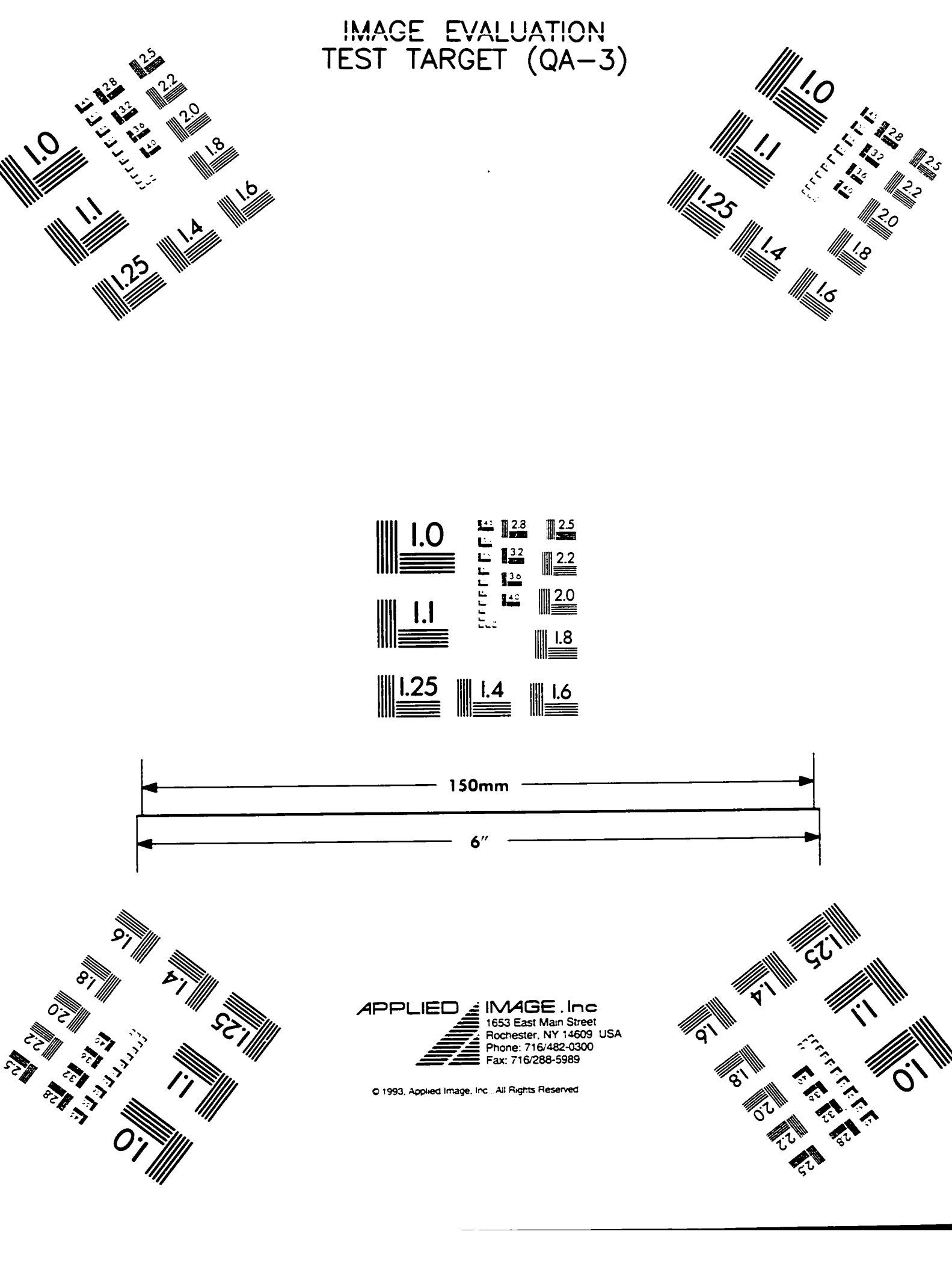
IMAGE EVALUATION
TEST TARGET (QA-3)
1.0
1.1
1.25
1.4
1.6
2.8
2.5
3.2
2.2
3.6
2.0
4.0
1.8
150mm
6"
APPLIED IMAGE, Inc
1653 East Main Street
Rochester, NY 14609 USA
Phone: 716/482-0300
Fax: 716/288-5989
© 1993, Applied Image, Inc. All Rights Reserved